

2018-02

Role of mTOR in autophagic and lysosomal reactions to environmental stressors in molluscs

Sforzini, S

<http://hdl.handle.net/10026.1/12353>

10.1016/j.aquatox.2017.12.014

Aquatic Toxicology

Elsevier

All content in PEARL is protected by copyright law. Author manuscripts are made available in accordance with publisher policies. Please cite only the published version using the details provided on the item record or document. In the absence of an open licence (e.g. Creative Commons), permissions for further reuse of content should be sought from the publisher or author.

1 **Role of mTOR in autophagic and lysosomal reactions to**
2 **environmental stressors in molluscs**

3
4 Susanna Sforzini ^{a,b}, Michael N. Moore ^{a,c,d,e}, Caterina Oliveri ^a, Anna Volta ^a, Awadhesh Jha ^e,
5 Mohamed Banni ^{a,f}, Aldo Viarengo ^{a,b}

6
7 ^a Department of Sciences and Technological Innovation (DiSIT), University of Piemonte Orientale
8 "A. Avogadro", V.le T. Michel 11, 15121 Alessandria, Italy

9 ^b Laboratory of Environmental Chemistry and Toxicology, IRCCS - Istituto di Ricerche
10 Farmacologiche Mario Negri, Via Giuseppe La Masa 19, 20156 Milan, Italy

11 ^c European Centre for Environment & Human Health (ECEHH), University of Exeter Medical
12 School, Truro, TR1 3HD, UK

13 ^d Plymouth Marine Laboratory, Plymouth, PL1 3DH, UK

14 ^e School of Biological and Marine Sciences, University of Plymouth, Drake Circus, Plymouth, PL4
15 8AA, UK

16 ^f Laboratory of Biochemistry and Environmental Toxicology, ISA, Chott-Mariem, Sousse, Tunisia

17
18 Corresponding author:

19 Aldo Viarengo

20 Department of Sciences and Technological Innovation (DiSIT), University of Piemonte Orientale
21 "A. Avogadro", V.le T. Michel 11, 15121 Alessandria, Italy

22 Phone: + 390131360370

23 Fax: +390131360390

24 e-mail: viarengo@uniupo.it

25

26 **Abstract**

27 Lysosomal membrane stability (LMS) has been used in various organisms as a very sensitive
28 biomarker of stress. However, despite the abundance of data about regulation of the autophagic
29 process in mammals, in the invertebrates there is only limited mechanistic understanding. Marine
30 mussels (*Mytilus galloprovincialis* Lam.) are bivalve molluscs, widely used as models in
31 ecotoxicology and as environmental bioindicators of sea water quality. In order to elucidate this
32 fundamental process, in the present study, mussels were exposed for 3 days to a “priority”,
33 ubiquitous environmental contaminant, benzo[*a*]pyrene (B[*a*]P) at different concentrations (i.e. 5,
34 50, 100 µg/L seawater). B[*a*]P accumulated in lysosomes of digestive tubule epithelial cells
35 (digestive cells) and in enlarged lipid-rich lysosomes (autolysosomes) as detected by
36 immunofluorescence and UV-fluorescence. B[*a*]P also activated the autophagic process with a
37 marked decrease of LMS and concurrent increase in lysosomal/cytoplasmic volume ratio.
38 Dephosphorylation of mTOR contributes to increased lysosomal membrane permeability and
39 induced autophagy. B[*a*]P induced a decrease in phosphorylated (active form) mTOR. The probable
40 role of mTOR in cell signalling and the regulation of the cellular responses to the contaminants has
41 been also confirmed in a field study, where there was significant inactivation of mTOR in stressed
42 animals. Statistical and network modelling supported the empirical investigations of autophagy and
43 mTOR; and was used to integrate the mechanistic biomarker data with chemical analysis and DNA
44 damage.

45

46 **Keywords:** mussel, autophagy, B[*a*]P, mTOR, network modelling

47

48 **1. Introduction**

49 Over the last decades, the studies about the biological effects of environmental stressors including
50 toxic chemicals have led to development of numerous biomarkers at different levels of functional
51 complexity suitable to follow the evolution of the stress syndrome from the early warning signals at
52 the molecular/cellular level to the deterioration at the organism level (Moore et al., 2012; Viarengo
53 et al., 2007). Among others, numerous lysosomal-related biomarkers have been developed;
54 lysosomes, highly conserved organelles playing a pivotal role in many cellular processes, were
55 shown to be the target for a wide range of contaminants (Appelqvist et al., 2013; Moore, 1988;
56 Moore et al., 2007; Viarengo and Nott, 1993). In particular, lysosomal membrane stability (LMS),
57 whose reduction represents a subcellular pathological reaction known to be linked to augmented
58 autophagic sequestration of cellular components, has been used both in invertebrates and
59 vertebrates as a very sensitive and easy to use biomarker of stress (Fernández et al., 2005; Moore et
60 al., 2004a; Sforzini et al., 2015; Svendsen et al., 2004).

61 Autophagy (i.e. macroautophagy), the major inducible pathway for general turnover of cytoplasmic
62 components, takes place in all eukaryotic cells (Klionsky and Emr, 2000). This process plays an
63 essential role in promoting cell survival in response to metabolic as well toxic stress by the
64 sequestration of cytoplasmic components, the removal of damaged organelles and protein
65 aggregates and their subsequent degradation in lysosomes. However, an excessive autophagic rate
66 has been shown to have deleterious consequences for tissue/organism health (Levine and Kroemer,
67 2008). Autophagy is well documented in marine mussels using biochemical, cell fractionation,
68 cytochemical and ultrastructural methods, where it is induced by many environmental stressors
69 including fasting, increased salinity, polycyclic aromatic hydrocarbons (PAHs) and chloroquine
70 (Bayne et al., 1980; Moore, 2004, 2008; Moore & Clarke, 1982; Moore et al., 1980, 1996, 2006a, b;
71 2007; Nott et al., 1985; Pipe & Moore, 1985).

72 Stress-induced autophagy, such as that induced by nutrient starvation, is regulated by the inhibition
73 of mTOR (mechanistic Target of Rapamycin) in eukaryotic cells from yeast to mammals (Klionsky
74 and Emr, 2000; Moore et al., 2012). mTOR is an evolutionarily-conserved serine/threonine protein
75 kinase that senses and integrates a variety of cellular physiological and environmental signals to
76 regulate cell growth (Jung et al., 2010). The phosphorylated active form of mTOR is involved in
77 various processes, such as activation of protein translation (transcription, ribosome biogenesis,
78 protein synthesis) and inhibition of the autophagic activity (Dowling et al., 2010; Soulard et al.,
79 2009). Despite the large number of studies on mammals demonstrating the existence of multiple
80 diverse regulators of mTOR and its involvement in the onset of several pathologies (Laplante and
81 Sabatini, 2012), the research on TOR signalling in invertebrates and in particular in contaminant
82 exposed organisms is an area where much remains to be explored (Soulard et al., 2009).

83 Molluscs are extensively used as models in many research fields (Abele et al., 2009; Gliński and
84 Jarosz, 1997); and are widely employed (in particular *Mytilus* sp.) as sentinel organisms in
85 biomonitoring programs (such as Med Pol, UNEP Mediterranean Biomonitoring Program; OSPAR
86 Convention; RA.MO.GE.; UNIDO) (Viarengo et al., 2007). The aim of this work was to investigate
87 the alterations of the lysosomal vacuolar system and the possible involvement of mTOR in their
88 regulation in the digestive gland of mussels *M. galloprovincialis* Lam. exposed to benzo[*a*]pyrene
89 (B[*a*]P), chosen as model organic xenobiotic. This toxic and genotoxic compound, priority pollutant
90 listed by U.S. EPA (Environmental Protection Agency) (U.S. EPA, 2009), is ubiquitous in the
91 environment and tends to persist and bioaccumulate through the food chain (Wang and Wang,
92 2006).

93 Following exposure to B[*a*]P, we investigated in mussel digestive gland (organ with storage and
94 distribution function; Bayne, 2009) firstly the accumulation and the subcellular distribution of
95 B[*a*]P, detected by immunofluorescence analysis using an anti-PAHs antibody. Moreover, in this
96 tissue, the effects on LMS and lysosomal/cytoplasmic (L/C) volume ratio, able to highlight the level

97 of stress in the organisms, from the early warning cellular signals (i.e. increased lysosomal
98 autophagic activity) to tissue pathology (i.e. excessive autophagy can trigger cell catabolism leading
99 to a loss of tissue functionality) were also measured. As a possible key element involved in the
100 regulation of the lysosomal activity, the role of the mTOR was evaluated by immunolabelling. The
101 level of mTOR phosphorylation was also investigated in mussels sampled in field from areas at
102 different levels of organic xenobiotic contamination.

103 Mathematical models provide the conceptual and mathematical formalism to integrate molecular,
104 cellular and whole animal processes (Allen & McVeigh, 2004; Allen & Moore, 2004; Moore &
105 Noble, 2004). Previous studies have shown that network complexity (as evaluated using network
106 connectedness -connectance CV%- and node size) can be used as an indicator of homeostasis or
107 health in cellular systems (Moore, 2010).

108 Modelling is essential for the derivation of explanatory frameworks that facilitates the development
109 of a predictive capacity for estimating outcomes or risk associated with particular disease processes
110 and stressful treatments (Moore, 2010; Moore & Noble, 2004; Moore et al., 2015). Previous studies
111 on mussels and earthworms have shown that there is a strong relationship between lysosomal
112 membrane stability (LMS), as an indicator of cellular health, and the responses of numerous stress
113 biomarkers (Moore et al., 2006a; Sforzini et al., 2015, 2017). In this investigation, principal
114 component analysis and network modelling was used to integrate multi-biomarker data; and to test a
115 predictive complexity model of cellular patho-physiological function.

116

117 **2. Materials and methods**

118 *2.1. Chemicals and organisms*

119 All chemicals were of analytical grade and purchased from Sigma-Aldrich Co. (UK/Italy), unless
120 otherwise indicated. Adult *Mytilus galloprovincialis* Lam. (50.7 ± 2.8 mm) were collected from the
121 intertidal zone at Trebarwith Strand, Cornwall, UK ($50^{\circ} 38' 40''$ N, $4^{\circ} 45' 44''$ W) in October 2014

122 (Banni et al, 2017). The site is relatively free of disease and is remotely located (Bignell et al.,
123 2011). Mussels were transported back to the laboratory in cool boxes and allowed to depurate for 7
124 days in natural seawater from Plymouth Sound. The seawater was maintained at 15.3 ± 0.68 °C and
125 filtered before to start the experiment ($\text{pH } 7.9 \pm 0.06$). During the depuration period, mussels were
126 fed with a suspension of *Isochrysis galbana* every 3 days (1.05×10^6 cells/mL), with a 100% water
127 change 2 h after each feeding.

128

129 2.2. *Experimental design and sampling*

130 After depuration, the mussels were transferred to 2-L glass beakers containing 1.8 L of the same
131 seawater as above and allowed to acclimatize for 48 h. The experiment began after this period and
132 consisted of a 3-day static exposure with no water changes, during which the mussels were not fed.
133 Two mussels were used per beaker. A photoperiod of 12 h light : 12 h dark was maintained
134 throughout the experiment. Good seawater oxygenation was provided by a bubbling system.
135 Seawater quality was monitored in each of the beakers by measuring salinity ($35.4 \pm 0.09\%$), pH
136 (7.9 ± 0.06), % dissolved oxygen ($97.9 \pm 3.22\%$) and temperature (15.3 ± 0.68 °C) (Banni et al.,
137 2017). Groups of mussels were exposed to four treatments i.e. solvent control (0.02% dimethyl
138 sulfoxide [DMSO]; 36 mussels); 5 µg/L B[a]P (36 mussels); 50 µg/L B[a]P (36 mussels); 100 µg/L
139 B[a]P (36 mussels). After 3 days exposure period, digestive glands were rapidly removed, placed
140 on aluminium cryostat chucks, chilled in super-cooled n-hexane and stored at -80 °C.
141 The B[a]P concentrations used in these experiments were selected taking into account that the levels
142 of PAHs in the sea water of contaminated environment range from 0.26 µg/L (Manodori et al.,
143 2006), 18.34 µg/L (Sinaei and Mashinchian, 2014) to 46 µg/L (Nasher et al., 2013). After 3 d of
144 exposure, the amount of chemical in the tissues of exposed animals was similar to that detected in
145 the tissues of mussels sampled in field contaminated coastal waters (Banni et al., 2017; Widdows et
146 al., 2002).

147

148 *2.3. Lysosomal alterations*

149 Frozen digestive gland sections (10 µm) of mussels from each exposure condition were cut by
150 cryostat (LeicaCM3050) and flash-dried by transferring them onto slides at room temperature.

151 Lysosomal membrane stability: The determination of LMS in the cells of the digestive gland was
152 performed on cryostat tissue sections following essentially the method described by Moore (1988).
153 This cytochemical assay is based on acid labilization characteristics of latent hydrolase β-*N*-
154 acetylhexosaminidase (NAH) using naphthol AS-BI-*N*-acetyl-β-D glucosaminide as a substrate for
155 NAH. Slides were observed using an inverted microscope (Zeiss Axiovert 100M) at 400 ×
156 magnification, connected to a digital camera (Zeiss AxioCam). The pictures obtained were analysed
157 using an image analysis system (Scion Image) that allowed for the determination of the labilisation
158 period i.e. the incubation time in the acid buffer needed to produce the maximal lysosomal staining.

159 Lysosomal/cytoplasmic (L/C) volume ratio: the L/C volume ratio of the digestive gland tissue was
160 evaluated following the method described by Moore (1976) and Moore and Clarke (1982).

161 Lysosomes were reacted for the lysosomal enzyme β-*N*-acetylhexosaminidase (NAH) using
162 naphthol AS-BI-*N*-acetyl-β-D glucosaminide as a substrate for NAH. The ratio between
163 cytoplasmic and lysosomal volumes was determined by analysing the images obtained from the
164 slides at 400 × magnification by image analysis as described above and expressed as a percentage
165 variation with respect to controls.

166

167 *2.4. Immunofluorescence analysis*

168 Cryostat frozen digestive gland sections (10 µm) obtained as described above were flash-dried by
169 transferring them onto poly-L-lysine-coated microscope slides at room temperature and fixed in
170 paraformaldehyde (PFA) solution (4% PFA in phosphate buffer saline-PBS, pH 7.2, 20 min at 20 ±
171 1 °C).

172 Immunofluorescent anti-PAHs staining was carried out as described by Sforzini et al., 2014.
173 Briefly, after fixation, sections were washed three times in PBS (5 min) and incubated in a
174 permeabilisation and blocking solution (0.5% Triton X-100, 2% bovine serum albumin-BSA, 0.5%
175 rabbit serum in PBS) for 1 h at 20 ± 1 °C. After rinsing, sections were incubated with the primary
176 antibody (monoclonal mouse anti-PAHs, Santa Cruz Biotechnology Inc., 1/100 in PBS containing
177 1% BSA and 0.05% Triton X-100) overnight at 4 °C in a moist chamber. Then, the sections were
178 washed (three times in PBS, 5 min) and the secondary antibody was applied i.e. polyclonal rabbit to
179 mouse IgG (FITC) (Abcam) (1/100 in 1% BSA and 0.05% Triton X-100 in PBS) for 1 h at 20 ± 1
180 °C in the dark. Sections were then rinsed in PBS, stained with DAPI (DNA-specific fluorescent
181 probe) and then mounted in Mowiol mounting medium (Cold Spring Harb Protoc, 2006).

182 Immunofluorescence colocalization of B[a]P and the lysosomal enzyme cathepsin D: following
183 immunolabelling with the first primary and secondary antibodies (as described above for single
184 labelling), sections were incubated for 1h at RT in PBS containing 2% BSA and 0.5% goat serum
185 (Sforzini et al., 2014). Hence, sections were incubated for 2h at 4°C with the second primary
186 antibody (rabbit polyclonal to cathepsin D (Abcam) 1/100 in PBS containing 1% BSA) and then,
187 after rinsing, in the secondary goat polyclonal to rabbit antibody (DyLight[®] 594, Abcam, 1/100 in
188 1% BSA in PBS, 1h, 20 ± 1 °C) in the dark. Finally, sections were then rinsed in PBS, stained with
189 DAPI and then mounted.

190 Immunofluorescent anti-mTOR phospho staining: sections prepared as described above were
191 incubated in a permeabilisation and blocking solution (0.5% Triton X-100, 2% BSA, 0.5% goat
192 serum in PBS, 1 h at 20 ± 1 °C) and then with the primary antibody (anti m-TOR (phospho S2448)
193 antibody, Abcam, 1/100 in PBS containing 1% BSA and 0.05% Triton X-100) overnight at 4 °C in
194 a moist chamber. Sections were then washed three times in PBS (5 min) and the secondary antibody
195 was applied, i.e. polyclonal goat to rabbit (Chromo) (Abcam) (1/100 in 1% BSA and 0.05% Triton

196 X-100 in PBS) for 1 h at 20 ± 1 °C in the dark. Finally, sections were rinsed in PBS, counterstained
197 with propidium iodide and mounted.

198 Immunofluorescent anti-mTOR staining: sections were incubated in a permeabilisation and
199 blocking solution as described above for the anti-mTOR phospho staining. Then, the primary
200 antibody (anti m-TOR antibody , Abcam, 1/200 in PBS containing 1% BSA and 0.05% Triton X-
201 100) was applied (overnight at 4 °C in a moist chamber). After washing in PBS, sections were
202 incubated with the secondary antibody, i.e. goat polyclonal to rabbit antibody (DyLight® 594)
203 (Abcam) (1/200 in 1% BSA and 0.05% Triton X-100 in PBS) for 1 h at 20 ± 1 °C in the dark.
204 Finally, sections were rinsed in PBS, counterstained with DAPI and mounted.

205 Controls for non-specific staining included sections that were processed in the absence of the
206 primary or secondary antibodies: no positive fluorescent stain was observed. Slides were viewed
207 under $400 \times$ magnification by an inverted photo-microscope (Zeiss Axiovert 100M connected to a
208 digital camera Zeiss AxioCam MRm) equipped for fluorescence microscopy using FITC,
209 Rhodamine and DAPI emission filters. Images were analysed using an image analysis system
210 (Scion Image) that allowed for the quantification of the mean fluorescence intensity. Sections
211 double immunolabelled for B[a]P and cathepsin D were viewed under $400 \times$ magnification by Axio
212 Observer and images were taken with ApoTome.2 (Zeiss, Germany).

213

214 *2.5. Sardinia samples and sampling sites: Field study*

215 Mussels (*M. galloprovincialis* Lam.), 4-5 cm in length, were obtained from a farm in Arborea (OR,
216 Sardinia, Italy) and kept in cages (240 mussels per site splitted in five bags) for 28 days (October-
217 November 2013) at three sites along the Sardinian coast: Porto Mannu li Fornelli ($40^{\circ}59'32.1''N$
218 $8^{\circ}12'54.5''E$ -reference site), Cala Reale ($41^{\circ}03'42.7''N$ $8^{\circ}17'17.5''E$ -a small marina), and Porto
219 Torres ($40^{\circ}50'23.1''N$ $8^{\circ}24'16.9''E$ -large industrial and commercial seaport). Mussels were caged in
220 polypropylene mesh bags placed about 4 m under the sea surface. At the end of the period of

221 caging, mussel digestive glands were excised, placed on aluminium cryostat chucks, chilled in
222 super-cooled n-hexane and stored at -80 °C. A large number of biomarkers have been measured in
223 digestive glands of mussels from the three sites; in this study, we investigated in these tissues the
224 response of mTOR.

225

226 *2.6. Univariate statistical analysis*

227 For B[a]P experiment, at least five replicates per control and per concentration were analysed. Each
228 replicate consists of the digestive gland from one mussel; the mussels were collected from a
229 separate beaker. For the field study, at least five replicates per caging site were analysed. Each
230 replicate consists of the digestive gland from one mussel; the mussels were collected from five
231 bags. The non-parametric Mann-Whitney *U*-test was used to compare the data from treated mussels
232 with those of the controls ones.

233

234 *2.7. Multivariate statistical analysis*

235 Biomarker data for mussels exposed to B[a]P were analysed using non-parametric multivariate
236 analysis software, PRIMER v 6 (PRIMER-E Ltd., Plymouth, UK; Clarke, 1999; Clarke &
237 Warwick, 2001). All data were log transformed [$\log_n(1+x)$] and standardised to the same scale.
238 Principal component analysis (PCA) and hierarchical cluster analysis, derived from Euclidean
239 distance similarity matrices were used to visualise dissimilarities between sample groups. The
240 results were further tested for significance using analysis of similarity (PRIMER v6 - ANOSIM),
241 which is an approximate analogue of the univariate ANOVA and reflects on differences between
242 treatment groups in contrast to differences among replicates within samples (the *R* statistic). Under
243 the null hypothesis H_0 (“no difference between samples”), $R = 0$ and this was tested by a non-
244 parametric permutations approach; there should be little or no effect on the average *R* value if the
245 labels identifying which replicates belong to which samples are randomly rearranged.

246 Finally, in order to map integrated biomarker data onto “health status space” (measured as system
247 complexity - connectance $C_v\%$) first principal components (PC1) for the biomarker data were
248 derived using PRIMER v6 and then plotted against the complexity values (as a measure of cellular
249 well-being) for each treatment (Allen and Moore, 2004; Moore et al., 2006a; Sforzini et al., 2015,
250 2017).

251

252 *2.8. Network modelling of biomarker data*

253 *2.8.1. Model description*

254 The generic cell model described by Moore (2010) has been developed from extensive published
255 data in the environmental toxicology and biomedical literature, and the large-scale organisation of
256 metabolic networks (Cuervo, 2004; Di Giulio & Hinton, 2008; Jeong et al., 2000; Klionsky & Emr,
257 2000). The generic cellular interaction network was constructed around the essential processes of
258 feeding, excretion and energy metabolism. Protein synthesis and degradation, including lysosomal
259 autophagy, are also incorporated in the model as are the major protective systems (Cuervo, 2004; Di
260 Giulio & Hinton, 2008; Livingstone et al., 2000; Moore, 2008; Moore et al., 2015). A modified
261 subset of the generic model was used in this investigation in order to accommodate the available
262 data (Fig. 8). The directed cellular physiological networks were constructed using Cytoscape 3.3.0
263 (Shannon et al., 2003).

264

265 *2.8.2. Analysis of cell system complexity*

266 Whole system complexity in the directed cellular physiological network was evaluated using
267 connectedness (Bonchev, 2003). Topological complexity was measured as connectedness or
268 connectance ($C_v\%$) is the ratio between the number of links E in the interaction network and the
269 number of links in the complete graph having the same number of nodes or vertices (V) (Bonchev,
270 2003). Connectedness relates the number of nodes (vertices) V and links or edges (arcs in a directed

271 link) E where the connectance ratio, C_V , of a directed graph (digraph) with V nodes or vertices is
272 then:

$$273 C_V = [(1 / \max(CV)) / \|E\|] \times 100$$

274 which reduces to: $C_V = (\|E\| / V^2) \times 100$

275 for typical digraphs that allow every node to connect to every other node, where $\|E\|$ is the nearest
276 integer function of E (Davis, 1997). This method uses the sum of the edge weights rather than the
277 edge count and allows for self-loops or arcs as with the autophagy process (Fig. 8).

278 Transformed biomarker data were used to attribute proportional weight values to the interactions
279 (edges) between cellular physiological processes (nodes) as shown in Table 1; and to the nodes, as
280 node size (Fig. 8). The various biomarker mean values were standardised to a proportion of Control
281 values. These standardised biomarker values (x) were used for biomarkers that normally decrease
282 with pathology (e.g., lysosomal membrane stability & mTORC1), while biomarkers that normally
283 increase with pathology (e.g., neutral lipid, lysosomal/cytoplasmic volume ratio & lipofuscin) were
284 further transformed to (x^{-1}). These values were normalised using \log_{10} transformation and then
285 inputted as the weight values for the network interactions (edges/links). The standardised biomarker
286 values were used to set node size for comparisons of network topology (see Fig. 8). The Kruskal-
287 Wallis test were applied to the proportional edge (interaction) values of the treatment groups.

288

289 **3. Results**

290 *3.1. Cytochemical and immunohistochemical analysis*

291 The concentrations of B[a]P utilised in this study, after 3 d of exposure, did not provoke any effect
292 on vitality of mussels (data not shown).

293 Immunofluorescence labelling of digestive glands of B[a]P exposed mussel with the anti-PAHs
294 antibody was positive (Fig. 1B-D); no immunopositivity was detected in control animals (Fig. 1A).

295 Double immunolabelling of sections with antibodies against PAHs and cathepsin D demonstrated

296 that B[a]P accumulated inside lysosomes (Fig. 1F). Quantification of the B[a]P fluorescence signal
297 by digital imaging (Fig. 1E) showed a significant increase in fluorescence intensity in animals
298 exposed to all the experimental conditions, with respect to controls; however, the most intense
299 staining was found at the lower B[a]P concentration (5 µg/L). The examination of unstained serial
300 sections of B[a]P exposed mussels under UV light highlighted the presence of numerous white-blue
301 fluorescent droplets; the fluorescence was minimal in the digestive glands of mussels exposed to 5
302 µg/L and increased from 50 µg/L to 100 µg/L B[a]P (Fig. 2).

303 B[a]P accumulated in the digestive glands of exposed mussels provoked significant alterations to
304 the lysosomal vacuolar system (Fig. 3). As shown in Fig. 3A, a decrease of LMS was observed at
305 all the concentrations, that was significant at 50 µg/L and 100 µg/L B[a]P. At the higher B[a]P
306 concentrations i.e. 50 µg/L and 100 µg/L B[a]P, a significant increase of the lysosomal/cytoplasmic
307 volume ratio, a biomarker of tissue damage, was also observed (+44% and +42% respectively, with
308 respect to controls) (Fig. 3B).

309 The use of an anti-mTOR antibody phosphorylated on S2448 revealed in digestive gland sections of
310 control mussels an immunopositive reaction; in particular, the fluorescence signal was mainly
311 located in the perinuclear region of the tubule epithelial cells (Fig. 4A). The immunohistochemical
312 data demonstrated that in the digestive gland cells of mussels exposed to all the different B[a]P
313 concentrations, the level of phosphorylated mTOR significantly decreased (Fig. 4F); stronger
314 effects were observed at 50 µg/L B[a]P and in particular at 100 µg/L B[a]P (Fig. 4C-E, F). The
315 specificity of this mTOR antibody within the mussel digestive gland was demonstrated by western
316 blot analysis; these results also confirm the dephosphorylation of the protein in B[a]P exposed
317 mussels (see Supplementary Information for the details of the method and western blot figure -Fig.
318 S1).

319 The results reported in Fig. 5 clearly demonstrate that mTOR protein level showed a strong increase
320 in the cytoplasm of the animals exposed to B[a]P, reaching the highest values in the digestive gland
321 of mussels treated with B[a]P 50-100 µg/L.

322 When the immunofluorescence staining with the anti-mTOR phosphorylated antibody was
323 performed in digestive gland sections of mussels caged along the Sardinian coast, the analysis
324 revealed a strong inactivation of mTOR in Porto Torres (a polluted areas) with respect to the
325 reference site (Porto Mannu li Fornelli) (Fig. 6A, C).

326

327 *3.2. Multivariate analysis of biomarker reactions*

328 Principal component (PCA) and hierarchical cluster analysis of all the biomarker reactions showed
329 that B[a]P had a detrimental effect on the digestive cells of mussels (Fig. 7). Analysis of similarity
330 shows that these clusters were significantly different (ANOSIM, R Statistic: $R = 0.856$, $P = 0.001$).
331 Treatments were clearly separated ($P < 0.01$) with the exceptions of the 50 and 100 µg/L, which
332 overlapped but were still significantly different ($P < 0.05$). Multiple regression analysis of the
333 biomarker data indicated that all of the biological parameters were significantly correlated ($P <$
334 0.01).

335

336 *3.3. Network modelling biomarker reactions to B[a]P treatment*

337 Inputting the biomarker data into the directed cellular interaction network (digraph) model (Fig. 8)
338 allowed the determination of the system complexity. Complexity values as connectance ratio (Cv%)
339 for the experimental treatments are shown in Fig. 8, with a considerable significant loss in
340 connectivity in the B[a]P treated conditions compared with the controls ($P = 5.52 \times 10^{-8}$, Kruskal-
341 Wallis test).

342 The control and treated network topologies differ in node size and are significantly different as
343 demonstrated by the ANOSIM and PCA/cluster analysis (Fig. 7). The determination of node degree

344 indicated that autophagy was the most highly connected node with 8 degrees (i.e., summation of 3
345 out-arc, 4 in-arcs and 1 loop), making it an important physiological hub (Fig. 8). System complexity
346 (connectance %) was strongly correlated with the concentration of B[a]P (inverse), lysosomal
347 stability (direct), first principal component (direct) and DNA damage (inverse; COMET assay data
348 from Banni et al, 2017; see also Canova et al, 1998) as shown in Fig. 9.

349

350 **4. Discussion**

351 In this study, we investigated the reactions of the lysosomal vacuolar system and the possible
352 involvement of mTOR in their regulation in the digestive gland of mussels *M. galloprovincialis*.
353 exposed to B[a]P. The digestive gland of bivalve mollusks is the principal site of digestion and
354 absorption (Bayne, 2009); and represents the major tissue involved in the accumulation and
355 detoxification of organic and inorganic environmental contaminants (Banni et al., 2016; Gomes et
356 al., 2012; Moore, et al., 2007; Viarengo et al., 1981). The lysosomal vacuolar system of the
357 digestive gland cells is well-developed, providing for most of the above mentioned functions
358 (Dimitriadis et al., 2004; Moore, 1988).

359 B[a]P accumulated in digestive tubule epithelial cells of exposed mussels, as revealed by
360 immunohistochemical analysis of digestive gland tissue sections by using an anti-PAHs antibody.
361 This method, recently developed in earthworm tissues (Sforzini et al., 2014), proved to be a reliable
362 tool for demonstrating the presence and the cellular distribution of B[a]P in animals exposed to
363 soils contaminated by even a minimal amount of this chemical (0.1 ppm). In particular, the use of
364 the double immunohistochemical method for co-localization of B[a]P and the cathepsin D (a
365 lysosomal protease highly conserved throughout lower and higher eukaryotes - Phillips et al., 2006)
366 demonstrated the lysosomal accumulation of the organic xenobiotic compound.

367 Interestingly, the fluorescence intensity was more intense in the digestive glands from mussels
368 exposed to the lowest B[a]P concentration (5 µg/L). Previous studies demonstrated that different

369 PAHs such as B[a]P and fluoranthene, when present in the tissues at high concentrations, are
370 progressively compartmentalised in lipid rich vesicles, with fluorescence properties (fluorescence
371 intensity directly related to the chemical amount) (Allison and Mallucci, 1964; Moore et al., 2007;
372 Plant et al., 1985; Sforzini et al., 2014). These chemicals are highly lipophilic and are known to
373 induce an alteration of fatty acid metabolism (lipidosis) (De Coster and van Larebeke, 2012; Moore
374 et al., 2007); lipids are then internalised into the lysosomes by autophagic uptake (Moore, 1988;
375 Podechard et al., 2009). In mussels exposed to all the different concentrations of B[a]P, a
376 significant increase was observed in lysosomal neutral lipid content of the digestive gland cells
377 (Fig. S2 - see Supplementary Information). The comparison between serial sections of tissues from
378 mussels exposed to B[a]P 50, 100 µg/L stained with Oil-Red O (lipid soluble dye commonly used
379 for the histochemical staining of neutral lipids in cryostat tissue sections -Bayliss High, 1984;
380 Moore, 1988) in bright-field and unstained sections by UV-fluorescence, highlighted that the
381 distribution of the B[a]P fluorescent droplets in the digestive gland cells corresponds to that of the
382 neutral lipid containing vesicles (Fig. 10). Recent studies have reported difficulty in labelling target
383 molecules in lipid droplets by immunofluorescence methods, probably because of the reduced
384 accessibility of these compartments to the antibodies (DiDonato and Brasaemle, 2003; Ohsaki et al.,
385 2005; Sforzini et al., 2014). Chemical results support this hypothesis, showing that the amount of
386 B[a]P accumulated in the digestive gland of exposed mussels increased with increasing dose; in
387 addition, the lipid concentration also increased with increasing exposure concentrations (Banni et
388 al., 2017).

389 Lysosomes of B[a]P exposed mussels showed relevant perturbations in their activity. LMS was
390 reduced in animals exposed to 5 µg/L B[a]P but stronger effects were observed at 50 and 100 µg/L.
391 Lysosomes are the target for many pollutants (both organic xenobiotics as well toxic metals); the
392 chemicals accumulated in lysosomes may perturb normal function and damage the lysosomal
393 membrane (Moore et al., 2006b; Sforzini et al., 2014; Viarengo et al., 1981). Pathological reactions

394 involving the lysosomal system are also often linked to augmented autophagic sequestration of
395 cytoplasmic components (e.g. autophagic accumulation of neutral lipids) and the removal of
396 damaged organelles and proteins (which are degraded in lysosomes) (Glick, et al., 2010; Moore,
397 2008). In vertebrates, quinone derivatives, produced during B[a]P metabolic processes, generate
398 reactive oxygen species (ROS) by redox cycling, which oxidatively altered DNA, protein, and
399 antioxidant enzymes (Kim and Lee, 1997). B[a]P is metabolized predominantly to quinones by
400 mussel digestive gland microsomes (Livingstone et al., 1988; Stegeman, 1985). Although the
401 hydrocarbon metabolism in molluscs is slow and the rate-limiting cytochrome P450 may be
402 responsible for this (Livingstone, 1998), previous studies have demonstrated changes in antioxidant
403 enzymes and peroxisomal proliferation with exposure of mussels to B[a]P (Livingstone et al., 1990;
404 Orbea et al., 2002), indicating an enhancement of oxyradical generation. In mussels exposed to all
405 the different concentrations of B[a]P utilised in this study, Banni et al. (2017) demonstrated an
406 increase of lipofuscin accumulated in lysosomes of digestive gland cells. It is likely that reactive
407 free radicals contribute to the damaging effects on the lysosomal membrane and build-up of
408 lipofuscin (end product of oxidative attack on lipids and proteins) (Viarengo, 1989; Moore, 2008;
409 Winston et al., 1996).

410 In this context, the autophagy may have a protective role in the context of (oxidative) stress through
411 the degradation and recycling of oxidised proteins and damaged organelles (Cuervo, 2004).
412 However, an excessive autophagic rate has been shown to have deleterious consequences for
413 tissue/organism health (Levine and Kroemer, 2008). At the higher B[a]P concentrations, a
414 significant enhancement of L/C volume ratio was also observed. These data indicate that the
415 animals are catabolic i.e. the autophagic process is highly stimulated and the catabolism of the
416 macromolecules is not compensated by protein synthesis. The (oxidative) damage to cellular
417 components may have contributed to decrease protein synthesis (Viarengo, 1989; Winston et al.,

418 1996; Moore et al., 2006a). The reduction of the cytoplasm of the cells may lead a loss of their
419 proper functionality with negative consequences on digestive gland physiology.

420 Overall, these results confirm that digestive cell lysosomes are the targets for toxic chemicals and
421 they are also sites of their accumulation. B[a]P stimulated the lysosomal fatty acid accumulation
422 and at the higher concentrations was stored in these compartments. Moreover, at the higher doses,
423 B[a]P also overstimulates the autophagic process leading to cell catabolism and thus tissue
424 pathology. One of the possible processes that could explain the observed effects is the mTOR signal
425 transduction pathway. mTOR (mechanistic target of rapamycin) is an evolutionarily-conserved
426 serine/threonine protein kinase that represents the central node of a highly conserved signalling
427 network regulating cell growth in response to nutrients, hormones and stresses (Jung et al., 2010).
428 mTOR is found in two functionally distinct complexes, mTORC1 and mTORC2. In particular, the
429 phosphorylated active form of TORC1 mediates temporal control of cell growth by activating
430 anabolic processes such as transcription, ribosome biogenesis, protein synthesis; and by inhibiting
431 catabolic processes such as autophagy (Dowling et al., 2010; Soulard et al., 2009). In mammals a
432 lot of studies have been devoted to investigate mTOR regulators. The dysregulation of mTOR
433 signalling is implicated in a number of human diseases including cancer (Dowling et al., 2010). In
434 invertebrates, the research on TOR signalling, particularly in contaminant exposed organisms is an
435 area where much remains to be explored (Soulard et al., 2009).

436 Recently, Copp et al. (2009) showed that mTOR is phosphorylated differentially when associated
437 with mTORC1 and mTORC2; specifically, they found that mTORC1 contains mTOR
438 phosphorylated predominantly on S2448. The immunofluorescence labelling of control digestive
439 gland sections using an anti-mTOR antibody phosphorylated on S2448 revealed an immunopositive
440 reaction; in particular, the fluorescence signal was mainly located in the perinuclear region of the
441 tubule epithelial cells. These results are in line with other studies showing that mTORC1 in
442 different kind of cells (such as trypanosomes, yeast and mammalian cells) localizes mainly to the

443 nucleus (Barquilla et al., 2008; Li et al., 2006). When the digestive gland cells of mussels exposed
444 to all the different B[a]P concentrations were reacted for the anti-mTOR (phospho S2448) antibody,
445 the fluorescent signal decreased; at 50 µg/L B[a]P and in particular at 100 µg/L B[a]P, i.e.
446 concentrations that provoked a sustained increase of the cellular catabolic rate, we observed
447 dramatic changes. Although the mechanisms that regulate the mTOR dephosphorylation are not till
448 now fully understood, the possibility that B[a]P stimulating ROS production may affect mTOR
449 activities is in line with recently reported results (Chen et al., 2010; Moore, 2008). It is important to
450 mention that the total amount of mTOR showed a significant increase in mussels exposed to the
451 different B[a]P concentrations (Fig. 5). This fact emphasises the importance of mTOR
452 phosphorylation/dephosphorylation in the regulation of cell metabolism.

453 An important aspect of this study was to investigate if the data obtained could have a general value,
454 i.e. if the level of phosphorylation of mTOR (activation/inhibition) could be also observed in
455 mussels exposed to field environmental conditions. To this end, we analysed mussels that were
456 caged for 28d in different sites along the Sardinian coast characterized by different levels of
457 contamination i.e. Fornelli, the reference site, Cala Reale, a small marina, and Porto Torres, large
458 industrial and commercial seaport contaminated by PAHs and heavy metals. An intense mTORC1
459 fluorescent signal was observed in the perinuclear area of the digestive gland cells of mussels caged
460 in the reference site (Fornelli); immunofluorescence staining showed a decrease in mussels caged in
461 Cala Reale. In mussels caged in Porto Torres, the level of mTOR phosphorylation was extremely
462 low; in the digestive glands of the same animals we have found a strong decrease of LMS and an
463 enhancement of L/C volume ratio; as well oxidative stress damage (Banni et al., manuscript in
464 preparation). The “picture” depicted by the field experiment is very similar to that observed in the
465 lab one.

466 Principal Component Analysis (PCA) is an effective method for integrating biomarker data into a
467 “health status space” reducing the multi-dimensionality of the problem to a simple two dimensional

468 representation (Chatfield and Collins, 1980; Allen and Moore, 2004). PCA is commonly used as a
469 cluster analysis tool and effectively captures the variability in a dataset in terms of principal
470 components, and previously PCA has facilitated modelling the integrated responses of multiple
471 biomarkers in the context of “health status space” (Allen and Moore, 2004; Moore et al., 2006a).
472 These models have shown that there is a strong relationship between LMS, as an indicator of
473 cellular health, and other combined biomarker responses (Allen & Moore, 2004; Moore et al.,
474 2006a; Sforzini et al., 2015, 2017).

475 However, PCA and cluster analysis does not integrate the various biomarkers in a functionally
476 meaningful way, and is only the first stage in developing numerical and network models for
477 environmental impact on the health of sentinel animals such as mussels and earthworms (Allen and
478 Moore, 2004; Moore, 2010; Sforzini et al., 2015, 2017). In order to encapsulate the cellular
479 physiological processes, it is necessary to interconnect the biomarker data into a logical framework.
480 This was done using a network model of the physiological/pathological processes known to occur in
481 the digestive cells. Complexity is a measure of the interconnectedness of the network and can be
482 used as an indicator of homeostasis (Lewis et al., 1992; Moore, 2010; Moore et al., 2015; Sedivy,
483 1999). Complexity of the whole system increases when sub-systems, such as detoxication and anti-
484 oxidant protective processes, augmented autophagy, protein degradation and induction of stress
485 proteins, are up-regulated and start to interact significantly as part of a response to low-level stress
486 (i.e., biphasic or hormetic response; Moore, 2010; Moore et al., 2015). However, with increasing
487 severity of stress, cell injury and higher-level functional impairment lead to physiological
488 dysfunction, pathology and breakdown of the whole interaction network with consequent loss of
489 complexity (Moore, 2010). Consequently, inputting the biomarker data from the B[a]P exposure
490 experiment into a directed cell physiology network model showed that there was a statistically
491 significant reduction in system complexity with increasing tissue B[a]P, indicating decreased
492 homeostasis and health status (Fig. 9; Table 1). Network topology was also significantly different in

493 terms of node size (Fig. 8). The model demonstrates that autophagy is an important highly
494 connected hub in the cellular physiology of the system being tested, which lends support to the
495 overall hypothesis, namely, that autophagy, lysosomal function and mTOR signaling are
496 intrinsically interlinked in responses/reactions to stress (Fig. 8). The strong correlations between
497 network complexity, B[a]P concentration, lysosomal stability and first principal component further
498 support the use of system complexity as a measure of cellular homeostasis (Fig. 9).

499 The network approach supports the hypothesis that stress leading to pathology results in a loss of
500 system complexity as previously described by Moore (2010). Consequently, cellular networks can
501 be used to integrate information from biomarker data; and to direct the selection of biomarkers and
502 design of experiments, in order to develop suites of tests that will demonstrate which links are
503 active or inactive, and to what degree. This provides mathematical formalism for an objective
504 evaluation of health status for potential use in risk assessment (Moore, 2002, Moore et al., 2004b).

505 Cellular interaction networks also have considerable potential for integrating multi-biomarker data
506 for evaluation of whole system “health status” (Moore, 2010). The strong correlation between
507 system complexity and DNA damage indicates that this type of modelling has potential for
508 predicting cellular pathological endpoints (Canova et al., 1998; Fig. 9).

509 Finally, the network model facilitates the development of a mechanistic framework that
510 encapsulates the interrelated patho-physiological processes that are involved in the cellular
511 reactions to the B[a]P. These processes are described diagrammatically in Figure 11, although all of
512 them are evolutionarily highly conserved, some are not yet confirmed to occur in molluscs (i.e.,
513 mTOR links with endocytosis and MDR/Pgp40 multi-drug resistance transporter). This diagram
514 shows the linkages between endocytotic uptake of B[a]P with natural particles, transfer to the
515 lysosomal system, where accumulation will be further facilitated by P-glycoprotein (MDR-Pgp40)
516 in the lysosomal membrane (Minier & Moore, 1996a, b; Yang et al., 2002). Accumulation of B[a]P
517 and lipid in the lysosomal compartment results in ROS generation and formation of lipofuscin

518 (stress or age pigment) (Brunk & Terman, 2002; Moore et al., 2006a). Oxidative stress may have a
519 positive feedback inhibiting mTORC1 and enhancing autophagy (Brunk & Terman, 2002; Chen et
520 al., 2010; Moore et al., 2006a, 2015). Inhibition of mTORC1 will also inhibit endocytosis,
521 lysosomal membrane stability and activate Pgp40 (Boya, 2012; Flinn & Backer, 2010; Jiang & Liu,
522 2008). The increased flux of ROS will also contribute to oxidative damage to DNA (Canova et al.,
523 1998); and enhanced autophagy may engulf portions of damaged and undamaged genomic material
524 through partial nuclear autophagy (Buckland-Nicks & Hodgson, 2005; Mochida et al., 2015).
525 Autophagy of nuclear DNA may contribute to autophagic and/or apoptotic cell death as a
526 pathological endpoint (Lowe, 1988); and may be protective against the development of digestive
527 gland tumours, which are extremely rare in molluscs (Khudoleï & Sirenko, 1977).

528

529 **5. Conclusions**

530 Overall, the data obtained in this work demonstrate that the signal transduction pathways linked to
531 mTOR (and in particular to mTORC1) could play an important role to determine the set of the
532 pathological effects that render the organisms “catabolic” and therefore no more able to sustain a
533 correct scope for growth. The probable role of mTOR in cell signalling and the regulation of the
534 cellular responses to the contaminants has been confirmed in a field study, where in the digestive
535 gland of mussels sampled from contaminated sites there was an inactivation of mTOR. Obviously,
536 as mentioned above, part of the shown effects (and others such as DNA damage) may depend on the
537 direct effect of the toxic chemical on the different cellular components. The analysis of the data by
538 the network connectedness demonstrates that autophagy, lysosomal function and mTOR signalling
539 are intrinsically interlinked in responses/reactions to stress. This network approach supports the
540 hypothesis that stress leading to pathology results in a loss of system complexity (Moore, 2010).
541 Cellular interaction networks also have considerable potential for integrating multi-biomarker data

542 for evaluation of whole system “health status” and for potential use in risk assessment (Moore,
543 2010).

544

545 **Acknowledgements**

546 This study was supported financially by Natural Environment Research Council (NERC), UK
547 (Grant No.NE/L006782/1; PI: ANJ).

548

549 **References**

550 Abele, D., Brey, T., Philipp, E., 2009. Bivalve models of aging and the determination of molluscan
551 lifespans. *Exp. Gerontol.* 44, 307-315.

552 Allen, J.I., McVeigh, A., 2004. Towards computational models of cells for environmental
553 toxicology. *J. Mol. Histol.* 35,697-706.

554 Allen, J.I., Moore, M.N., 2004. Environmental prognostics: is the current use of biomarkers
555 appropriate for environmental risk evaluation. *Mar. Environ. Res.* 58, 227-232.

556 Allison, A.C., Mallucci, L., 1964. Uptake of hydrocarbon carcinogens by lysosomes. *Nature* 203,
557 1024-1027.

558 Appelqvist, H., Wäster, P., Kågedal, K., Öllinger, K., 2013. The lysosome: from waste bag to
559 potential therapeutic target. *J. Mol. Cell. Biol.* 5, 214-226.

560 Banni, M., Sforzini, S., Balbi, T., Corsi, I., Viarengo, A., Canesi, L., 2016. Combined effects of n-
561 TiO₂ and 2,3,7,8-TCDD in *Mytilus galloprovincialis* digestive gland: A transcriptomic and
562 immunohistochemical study. *Environ Res.* 145, 135-144.

563 Banni, M., Sforzini, S., Arlt, V. M., Barranger, A., Dallas, L. J., Oliveri, C., Aminot, Y., Pacchioni,
564 B., Millino, C., Lanfranchi, G., Readman, J. W., Moore, M. N., Viarengo, A., Jha, A. N.,
565 2017. Assessing the impact of Benzo[a]pyrene on Marine Mussels: Application of a novel

566 targeted low density microarray complementing classical biomarker responses. PLoS ONE
567 12(6), e0178460. <https://doi.org/10.1371/journal.pone.0178460>.

568 Barquilla, A., Crespo, J.L., Navarro, M.; 2008. Rapamycin inhibits trypanosome cell growth by
569 preventing TOR complex 2 formation. Proc. Natl. Acad. Sci. U S A 105,14579-14584.

570 Bayliss High, O., 1984. Lipid Histochemistry (Royal Microscopical Society, Microscopy
571 Handbooks, No. 6). Oxford University Press, Oxford.

572 Bayne, B.L., Moore, M.N. and Koehn, R.K., 1980. Lysosomes and the response by *Mytilus edulis*
573 to an increase in salinity. Mar. Biol. Letters 2, 193-204.

574 Bayne, B.L., 2009. Marine Mussels: Their Ecology and Physiology, Cambridge University Press,
575 528 p.

576 Bignell, J.P., Stentiford, G.D., Taylor, N. G., Lyons, B.P., 2011. Histopathology of mussels
577 (*Mytilus* sp.) from the Tamar Estuary, UK. Mar. Environ. Res. 72, 25-32.

578 Bonchev, D., 2003. Complexity of protein-protein interaction networks, complexes, and pathways.
579 In: Handbook of proteomic methods (Ed PM Conn) pp 451-462. Humana Press, Totowa, New
580 Jersey.

581 Boya, P., 2012. Lysosomal function and dysfunction: mechanism and disease. Antiox. Redox
582 Signaling 17, 766-774.

583 Brunk, U.T., Terman, A., 2002. Lipofuscin: mechanisms of age-related accumulation and influence
584 on cell function. Free Rad. Biol. Med. 33, 11-619.

585 Buckland-Nicks, J., Hodgson, A.N., 2005. Paraspermatogenesis of cerithioidean snails: retention of
586 an acrosome and nuclear remnant. J. Morphology 264, 314-326.

587 Canova, S., Degan, P., Peters, L.D., Livingstone, D.R., Voltan, R., Venier, P., 1998. Tissue dose,
588 DNA adducts, oxidative DNA damage and CYP1A-immunopositive proteins in mussels
589 exposed to waterborne benzo[a]pyrene. Mutation Res/Fundamental and Molecular
590 Mechanisms of Mutagenesis 399, 17-30.

591 Chatfield, C., Collins, A.J., 1980. Introduction to Multivariate Analysis. Chapman and Hall,
592 London.

593 Chen, L., Xu, B., Liu, L., Luo, Y., Yin, J., Zhou, H., Chen, W., Shen, T., Han, X., Huang, S., 2010.
594 Hydrogen peroxide inhibits mTOR signaling by activation of AMPKa leading to apoptosis of
595 neuronal cells. *Lab. Invest.* 90, 762-773.

596 Clarke, K.R., 1999. Non-metric multivariate analysis in community-level ecotoxicology. *Environ.*
597 *Toxicol. Chem.* 18, 117-127.

598 Clarke, K.R., Warwick, R.M., 2001. Change in marine communities: an approach to statistical
599 analysis and interpretation. PRIMER-*c*, Plymouth, UK.

600 Cold Spring Harb Protoc, 2006. doi: 10.1101/pdb.rec10255.

601 Copp, J., Manning, G., Hunter, T., 2009. TORC-specific phosphorylation of mammalian target of
602 rapamycin (mTOR): phospho-Ser2481 is a marker for intact mTOR signaling complex 2.
603 *Cancer Res.* 69, 1821-1827.

604 Cuervo, A.M., 2004. Autophagy: in sickness and in health. *TRENDS Cell Biol.* 14, 70-77.

605 Davis, M.W., 1997. Complexity formalisms, order and disorder in the structure of art. In:
606 Evolutionary Programming VI, Lecture Notes in Computer Science (Editors: Angeline PJ,
607 Reynolds, McDonnell JR, Eberhart R), Vol. 1213, Springer International Publishing AG,
608 Switzerland. pp 1-12.

609 De Coster, S., van Larebeke, N., 2012. Endocrine-disrupting chemicals: associated disorders and
610 mechanisms of action. *J. Environ. Public Health* 2012:713696.

611 Di Giulio, R.T., Hinton, D.E., Editors, 2008. The toxicology of fishes. Taylor and Francis, London,
612 New York, Singapore, Melbourne, 1071 p.

613 DiDonato, D., Brasaemle, D.L., 2003. Fixation methods for the study of lipid droplets by
614 immunofluorescence microscopy. *J. Histochem. Cytochem.* 51, 773-780.

615 Dimitriadis, V.K., Domouhtsidou, G.P., Cajaraville, M.P., 2004. Cytochemical and histochemical
616 aspects of the digestive gland cells of the mussel *Mytilus galloprovincialis* (L.) in relation to
617 function. *J. Mol. Histol.* 35, 501-509.

618 Dowling, R.J., Topisirovic, I., Fonseca, B.D., Sonenberg, N., 2010. Dissecting the role of mTOR:
619 lessons from mTOR inhibitors. *Biochim. Biophys. Acta* 1804, 433-439.

620 Fernández, F.P., Labrador, V., Pérez Martín, J.M., Hazen, M.J., 2005. Cytotoxic effects in
621 mammalian Vero cells exposed to pentachlorophenol. *Toxicology* 210, 37-44.

622 Flinn, R.J., Backer, J.M., 2010. mTORC1 signals from late endosomes: taking a TOR of the
623 endocytic system. *Cell Cycle*, 9, 1869-1870.

624 Glick, D., Barth, S., Macleod, K. F., 2010. Autophagy: cellular and molecular mechanisms. *J.*
625 *Pathol.* 221, 3-12.

626 Gliński, Z., Jarosz, J., 1997. Molluscan immune defenses. *Arch. Immunol. Ther. Exp. (Warsz)*. 45,
627 149-155.

628 Gomes, T., Pereira, C.G., Cardoso, C., Pinheiro, J.P., Cancio, I., Bebianno, M.J., 2012.
629 Accumulation and toxicity of copper oxide nanoparticles in the digestive gland of *Mytilus*
630 *galloprovincialis*. *Aquat Toxicol.* 118-119, 72-79.

631 Jeong, H., Tombor, B., Albert, R., Oltval, Z.N., Barábasi, A.-L., 2000. The large scale organization
632 of metabolic networks. *Nature* 407, 651-654.

633 Jiang, B.H., Liu, L.Z., 2008. Role of mTOR in anticancer drug resistance: perspectives for
634 improved drug treatment. *Drug Resist. Updates* 11, 63-76.

635 Jung, C.H., Ro, S.H., Cao, J., Otto, N.M., Kim, D.H., 2010. mTOR regulation of autophagy. *FEBS*
636 *Lett.* 584, 1287-1295.

637 Khudolei, V.V., Sirenko, O.A., 1977. Development of tumors in *Unio pictorum* bivalve mollusks
638 under the influence of N-nitroso compounds. *Biulleten'eksperimental'noi biologii i meditsiny*
639 83, 577-579.

640 Kim, K.B., Lee, B.M., 1997. Oxidative stress to DNA, protein, and antioxidant enzymes
641 (superoxide dismutase and catalase) in rats treated with benzo(a)pyrene. *Cancer Lett.* 113,
642 205-212.

643 Klionsky, D.J., Emr, S.D., 2000. Autophagy as a regulated pathway of cellular degradation. *Science*
644 290, 1717-1721.

645 Laplante, M., Sabatini, D. M., 2012. mTOR signaling in growth control and disease. *Cell.* 149, 274-
646 293.

647 Levine, B., Kroemer, G., 2008. Autophagy in the Pathogenesis of Disease. *Cell.* 132, 27-42.

648 Lewis, A., Lipsitz, M.D., Ary, L., Goldberger, M.D., 1992. Loss of “complexity” and aging:
649 potential applications of fractals and chaos theory to senescence. *J. Amer. Med. Assoc.* 267,
650 1806-1809.

651 Li, H., Tsang, C.K., Watkins, M., Bertram, P.G., Zheng, X.F., 2006. Nutrient regulates Tor1 nuclear
652 localization and association with rDNA promoter. *Nature* 442, 1058-1061.

653 Livingstone, D.R., 1998. The fate of organic xenobiotics in aquatic ecosystems: quantitative and
654 qualitative differences in biotransformation by invertebrates and fish. *Comp. Biochem.*
655 *Physiol. A Mol. Integr. Physiol.* 120, 43-49.

656 Livingstone, D.R., Garcia Martinez, P., Stegeman, J.J, Winston, G.W., 1988. Benzo[a]pyrene
657 metabolism and aspects of oxygen radical generation in the common mussel, *Mytilus edulis*.
658 *Biochem. Soc. Trans.* 16, 779.

659 Livingstone, D.R., Garcia Martinez, P., Michel, X., Narbonne, J. F., O'Hara, S., Ribera, D.,
660 Winston, G.W., 1990. Oxyradical Production as a Pollution-Mediated Mechanism of Toxicity
661 in the Common Mussel, *Mytilus edulis* L., and Other Molluscs. *Functional Ecology* Vol. 4,
662 No. 3, *New Horizons in Ecotoxicology*, pp. 415-424.

663 Livingstone, D.R., Chipman, J.K., Lowe, D.M., Minier, C., Mitchelmore, C.L., Moore, M.N.,
664 Peters, L.D., Pipe, R.K., 2000. Development of biomarkers to detect the effects of organic

665 pollution on aquatic invertebrates: recent molecular, genotoxic, cellular and immunological
666 studies on the common mussel (*Mytilus edulis* L.) and other mytilids. Int. J. Environ. Pollut.
667 13, 56-91.

668 Lowe, D.M., 1988. Alterations in cellular structure of *Mytilus edulis* resulting from exposure to
669 environmental contaminants under field and experimental conditions. Mar. Ecol. Prog. Ser.
670 46, 91-100.

671 Manodori, L., Gambaro, A., Piazza, R., Ferrari, S., Stortini, A.M., Moret, I., Capodaglio, G., 2006.
672 PCBs and PAHs in sea-surface microlayer and sub-surface water samples of the Venice
673 Lagoon (Italy). Mar. Pollut. Bull. 52, 184-192.

674 Minier, C., Moore, M.N., 1996a. Multixenobiotic resistance in mussel blood cells. Mar. Environ.
675 Res. 42, 389-392.

676 Minier, C., Moore, M.N., 1996b. Rhodamine B accumulation and MXR protein expression in
677 mussel blood cells: effects of exposure to vincristine. Mar. Ecol. Prog. Ser. 142, 165-173.

678 Mochida, K., Oikawa, Y., Kimura, Y., Kirisako, H., Hirano, H., Ohsumi, Y., Nakatogawa, H.,
679 2015. Receptor-mediated selective autophagy degrades the endoplasmic reticulum and the
680 nucleus. Nature 522, 59-362.

681 Moore, M.N., 1976. Cytochemical demonstration of latency of lysosomal hydrolases in digestive
682 gland cells of the common mussel *Mytilus edulis*, and changes induced by thermal stress. Cell
683 Tissue Res. 175, 279-287.

684 Moore, M.N., 1988. Cytochemical responses of the lysosomal system and NADPH-
685 ferrihemoprotein reductase in molluscan digestive cells to environmental and experimental
686 exposure to xenobiotics. Mar. Ecol. Prog. Ser. 46, 81-89.

687 Moore, M.N., 2002. Biocomplexity: the post-genome challenge in ecotoxicology. Aquat. Toxicol.
688 59, 1-15.

689 Moore, M.N., 2004. Diet restriction induced autophagy: a novel protective system against
690 oxidative- and pollutant-stress and cell injury. *Mar. Environ. Res.* 58, 603-607.

691 Moore, M.N., 2008. Autophagy as a second level protective process in conferring resistance to
692 environmentally-induced oxidative stress. *Autophagy* 4, 254-256.

693 Moore, M.N., 2010. Is toxicological pathology characterised by a loss of system complexity? *Mar.*
694 *Environ. Res.* 69, S37-S41.

695 Moore, M.N., Clarke, K.R., 1982. Use of microstereology and cytochemical staining to determine
696 the effects of crude oil-derived aromatic hydrocarbons on lysosomal structure and function in
697 a marine bivalve mollusc *Mytilus edulis*. *Histochem. J.* 14, 713-718.

698 Moore, M.N., Noble, D., 2004. Computational modelling of cell & tissue processes and function. *J.*
699 *Mol. Histol.* 35, 655-658.

700 Moore, M.N., Koehn R.K. and Bayne, B.L., 1980. Leucine aminopeptidase (aminopeptidase-1), N-
701 acetyl- β -hexosaminidase and lysosomes in the mussel *Mytilus edulis* L., in response to salinity
702 changes. *J. Exp. Zool.* 214, 239-249.

703 Moore, M.N., Soverchia, C. and Thomas, M., 1996. Enhanced lysosomal autophagy of intracellular
704 proteins by xenobiotics in living molluscan blood cells. In: *Proc. 10 th International Congress*
705 *Histochem. Cytochem., Acta Histchem. Cytochem.*, 29 (Supplement), 947-948.

706 Moore, M.N, Lowe, D.M., Kohler, A., 2004a. Biological effects of contaminants: Measurements of
707 lysosomal membrane stability. *ICES Techniques in Marine Environmental Sciences (TIMES)*,
708 vol. 36. ICES, Copenhagen.

709 Moore, M.N., Depledge, M.H., Readman, J.W., Leonard, P., 2004b. An integrated biomarker-based
710 strategy for ecotoxicological evaluation of risk in environmental management. *Mutat. Res.*
711 552, 247-268.

712 Moore, M.N., Allen, J.I., McVeigh, A., 2006a. Environmental prognostics: an integrated model
713 supporting lysosomal stress responses as predictive biomarkers of animal health status. Mar.
714 Environ. Res. 61, 278-304.

715 Moore, M.N., Allen, J.I., McVeigh, A., Shaw, J., 2006b. Lysosomal and autophagic reactions as
716 predictive indicators of environmental impact in aquatic animals. Autophagy 2, 217-220.

717 Moore, M.N., Viarengo, A., Donkin, P., Hawkins, A.J., 2007. Autophagic and lysosomal reactions
718 to stress in the hepatopancreas of blue mussels. Aquat. Toxicol. 84, 80-91.

719 Moore, M.N., Viarengo, A., Somerfield, P.J., Sforzini, S., 2012. Linking lysosomal biomarkers and
720 ecotoxicological effects at higher biological levels, in: Amiard-Triquet, C., Amiard, J.C.,
721 Rainbow, P.S. (Eds.), Ecological Biomarkers: Indicators of Ecotoxicological Effects. CRC
722 Press, Taylor & Francis Group, Boca Raton, FL, pp. 107-130.

723 Moore, M.N., Shaw, J.P., Ferrar Adams, D.R., Viarengo, A., 2015. Anti-oxidative cellular
724 protection effect of fasting-induced autophagy as a mechanism for hormesis. Mar. Environ.
725 Res. 107, 35-44.

726 Nasher, E., Heng, L.Y., Zakaria, Z., Surif, S., 2013. Concentrations and Sources of Polycyclic
727 Aromatic Hydrocarbons in the Seawater around Langkawi Island, Malaysia. Journal of
728 Chemistry. DOI: 10.1155/2013/975781.

729 Nott, J.A., Moore, M.N., Mavin, L.J. and Ryan, K.P., 1985. The fine structure of lysosomal
730 membranes and endoplasmic reticulum in the digestive gland of *Mytilus edulis* exposed to
731 anthracene and phenanthrene. Mar. Environ. Res. 17, 226-229.

732 Ohsaki, Y., Maeda, T., Fujimoto, T., 2005. Fixation and permeabilization protocol is critical for the
733 immunolabeling of lipid droplet proteins. Histochem. Cell Biol. 124, 445-452.

734 Orbea, A., Ortiz-Zarragoitia, M., Cajaraville, M.P., 2002. Interactive effects of benzo(a)pyrene and
735 cadmium and effects of di(2-ethylhexyl) phthalate on antioxidant and peroxisomal enzymes

736 and peroxisomal volume density in the digestive gland of mussel *Mytilus galloprovincialis*
737 Lmk. Biomarkers 7, 33-48.

738 Phillips, S.N., Muzaffar, N., Codlin, S., Korey, C.A., Taschner, P.E., de Voer, G., Mole, S.E.,
739 Pearce, D.A., 2006. Characterizing pathogenic processes in Batten disease: use of small
740 eukaryotic model systems. Biochim. Biophys. Acta 1762, 906–919.

741 Pipe, R.K. and Moore, M.N., 1985. Ultrastructural changes in the lysosomal-vacuolar system in
742 digestive cells of *Mytilus edulis* as a response to increased salinity. Mar. Biol. 87, 157-163.

743 Plant, A.L., Benson, D.M., Smith, L.C., 1985. Cellular uptake and intracellular localization of
744 benzo(a)pyrene by digital fluorescence imaging microscopy. J. Cell Biol. 100, 1295-1308.

745 Podechard, N., Le Ferrec, E., Rebillard, A., Fardel, O., Lecureur, V., 2009. NPC1 repression
746 contributes to lipid accumulation in human macrophages exposed to environmental aryl
747 hydrocarbons. Cardiovasc. Res. 82, 361-370.

748 Sedivy, R., 1999. Chaodynamic loss of complexity and self-similarity cancer. Med. Hypotheses 52,
749 271-274.

750 Sforzini, S., Moore, M.N., Boeri, M., Benfenati, E., Colombo, A., Viarengo, A., 2014.
751 Immunofluorescence detection and localization of B[a]P and TCDD in earthworm tissues.
752 Chemosphere 107, 282-289.

753 Sforzini, S., Moore, M.N., Boeri, M., Bencivenga, M., Viarengo, A., 2015. Effects of PAHs and
754 dioxins on the earthworm *Eisenia andrei*: a multivariate approach for biomarker
755 interpretation. Environ. Pollut. 196, 60-71.

756 Sforzini, S., Moore, M.N., Mou, Z., Boeri, M., Banni, M., Viarengo, A., 2017. Mode of action of
757 Cr(VI) in immunocytes of earthworms: Implications for animal health. Ecotox. Environ. Saf.
758 138, 298-308.

759 Shannon, P., Markiel, A., Ozier, O., Baliga, N.S., Wang, J.T., Ramage, D., Amin, N., Schwikowski,
760 B., Ideker, T., 2003. Cytoscape: a software environment for integrated models of biomolecular
761 interaction networks. *Genome Res.* 13, 2498-2504.

762 Sinaei, M., Mashinchian, A., 2014. Polycyclic aromatic hydrocarbons in the coastal sea water, the
763 surface sediment and Mudskipper *Boleophthalmus dussumieri* from coastal areas of the
764 Persian Gulf: source investigation, composition pattern and spatial distribution. *J. Environ.*
765 *Health Sci. Eng.* 12(1):59. doi: 10.1186/2052-336X-12-59.

766 Soulard, A., Cohen, A., Hall, M.N., 2009. TOR signaling in invertebrates. *Curr. Opin. Cell Biol.* 21,
767 825-836.

768 Stegeman, J.J., 1985. Benzo[a]pyrene oxidation and microsomal enzyme activity in the mussel
769 (*Mytilus edulis*) and other bivalve mollusc species from the Western North Atlantic. *Marine*
770 *Biology* 89, 21-39.

771 Svendsen, C., Spurgeon, D.J., Hankard, P.K., Weeks, J.M., 2004. A review of lysosomal membrane
772 stability measured by neutral red retention: is it a workable earthworm biomarker? *Ecotoxicol.*
773 *Environ. Saf.* 57, 20-29.

774 U.S. EPA (Environmental Protection Agency), Appendix A to 40 CFR, Part 423-126 Priority
775 Pollutants, 2009.

776 Viarengo, A., 1989. Heavy metals in marine invertebrates: mechanisms of regulation and toxicity at
777 the cellular level. *Rev. Aquat. Sci.* 1, 295-317.

778 Viarengo, A., Nott, J.A., 1993. Mini-review: Mechanisms of heavy metal cation homeostasis in
779 marine invertebrates. *Comp. Biochem. Physiol. C* 104, 355-372.

780 Viarengo, A., Zanicchi, G., Moore, M.N., Orunesu, M., 1981. Accumulation and detoxication of
781 copper by the mussel *Mytilus galloprovincialis* Lam.: A study of the subcellular distribution in
782 the digestive gland cells. *Aquat. Toxicol.* 1, 147-157.

783 Viarengo, A., Lowe, D., Bolognesi, C., Fabbri, E., Koehler, A., 2007. The use of biomarkers in
784 biomonitoring: a 2-tier approach assessing the level of pollutant-induced stress syndrome in
785 sentinel organisms. *Comp. Biochem. Physiol. C* 146, 281-300.

786 Wang, X., Wang, W.-X., 2006. Bioaccumulation and transfer of benzo(a)pyrene in a simplified
787 marine food chain. *Mar. Ecol. Prog. Ser.* 312, 101-111.

788 Widdows, J., Donkin, P., Staff, F.J., Matthiessen, P., Law, R.J., Allen, Y.T., Thain, J.E., Allchin,
789 C.R., Jones, B.R., 2002. Measurement of stress effects (scope for growth) and contaminant
790 levels in mussels (*Mytilus edulis*) collected from the Irish Sea. *Mar. Environ. Res.* 53, 327-
791 356.

792 Winston, G.W., Moore, M.N., Kirchin, M.A., Soverchia, C., 1996. Production of reactive oxygen
793 species (ROS) by hemocytes from the marine mussel, *Mytilus edulis*. *Comp. Biochem.*
794 *Physiol.* 113C, 221-229.

795 Yang, Y., Liu, X., Zhang, X.X., Korenaga, T., 2001. Study on the dynamic complexation between
796 protein and PAHs by capillary electrophoresis. *Analyt. Sciences* 2001 17(ICAS2001): i1345-
797 i1349.

798

799 **Table 1. Network model interactions and corresponding biomarker used for ascribing**
 800 **interaction strength.**

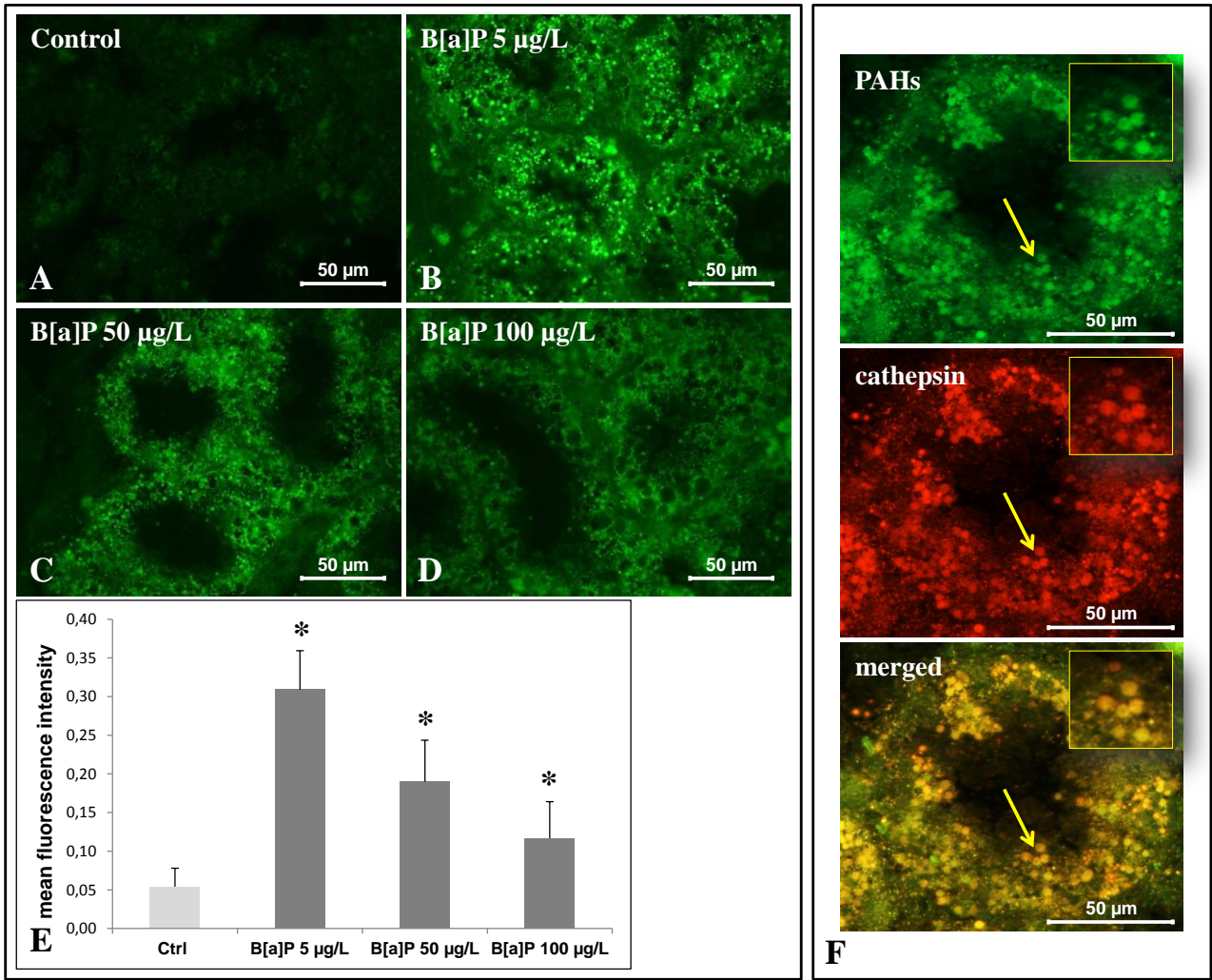
801

| <i>Interaction</i> | <i>Biomarker</i> |
|---------------------|---|
| LYS-AUT | Lysosomal Membrane Stability (LMS) |
| LYS-OxSt | Lysosomal Membrane Stability (LMS) |
| AUT-LYS | Lysosomal -Cytoplasmic Volume Ratio (Lys/Cyt Vol) |
| AUT-OxSt | Lysosomal -Cytoplasmic Volume Ratio (Lys/Cyt Vol) |
| AUT-AUT | Lysosomal -Cytoplasmic Volume Ratio (Lys/Cyt Vol) |
| AUT-DNA dam | Lysosomal -Cytoplasmic Volume Ratio (Lys/Cyt Vol) |
| LIPID-LYS | Neutral Lipid (NL) |
| LIPID-AUT | Neutral Lipid (NL) |
| mTORC1-LYS | mTORC1 (mTOR) |
| mTORC1-AUT | mTORC1 (mTOR) |
| OxSt-AUT | Lipofuscin (LF) |
| OxSt-LYS | Lipofuscin (LF) |
| OxSt-LIPID | Lipofuscin (LF) |
| OxSt-mTOR | Lipofuscin (LF) |
| OxSt-DNA dam | Lipofuscin (LF) |

802

803 **LYS – Lysosomal function; AUT – Autophagy; OxSt – Oxidative stress; DNA dam – DNA damage;**
 804 **Lipid – Neutral lipid (triglyceride); mTORC1 – Mechanistic target of rapamycin complex 1.**

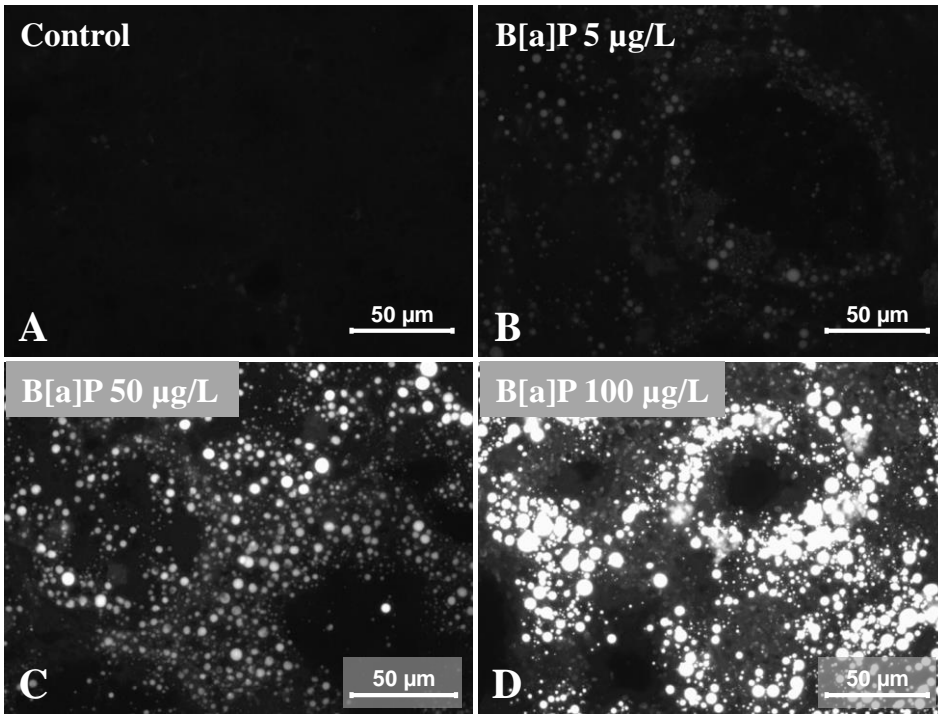
805



806

807 Fig. 1.

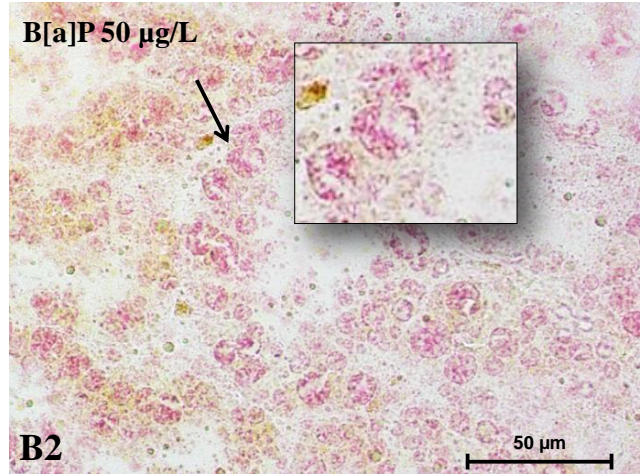
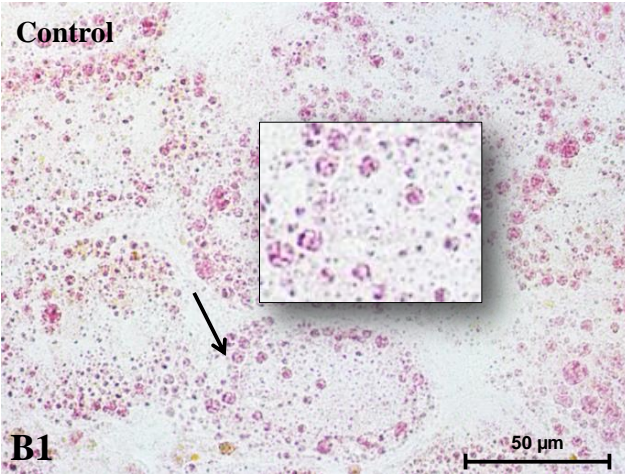
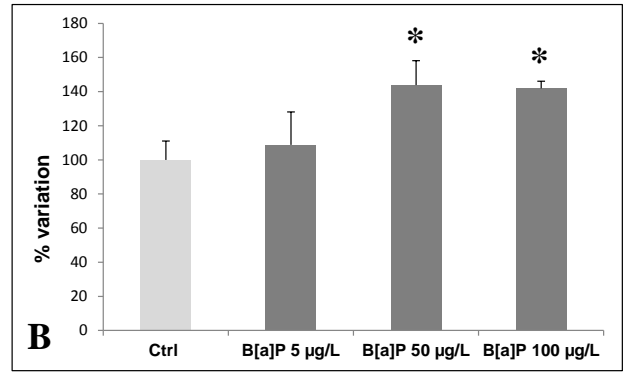
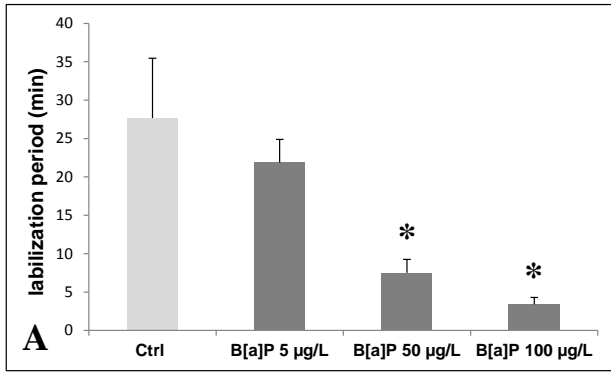
808



809

810 Fig. 2.

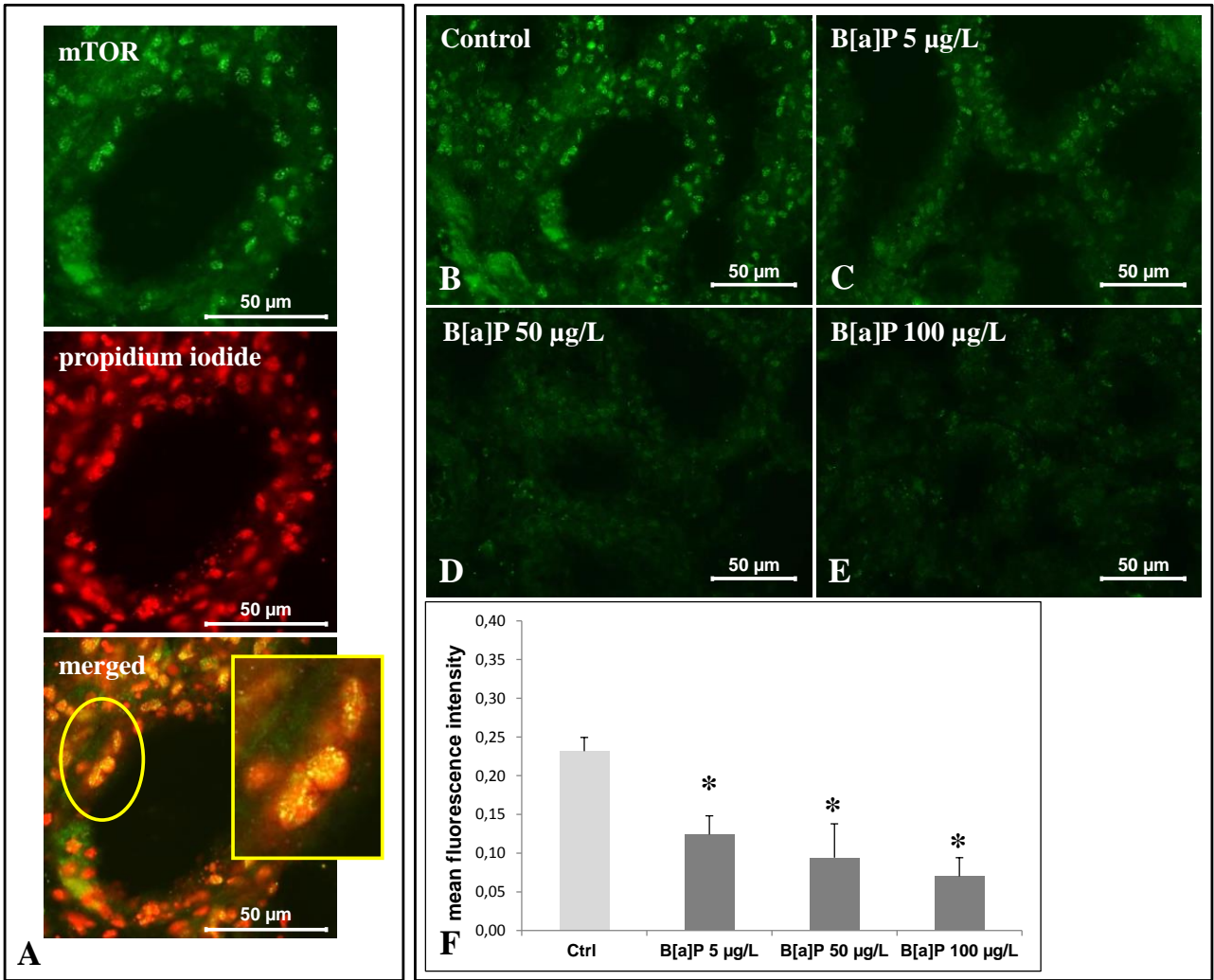
811



812

813 Fig. 3.

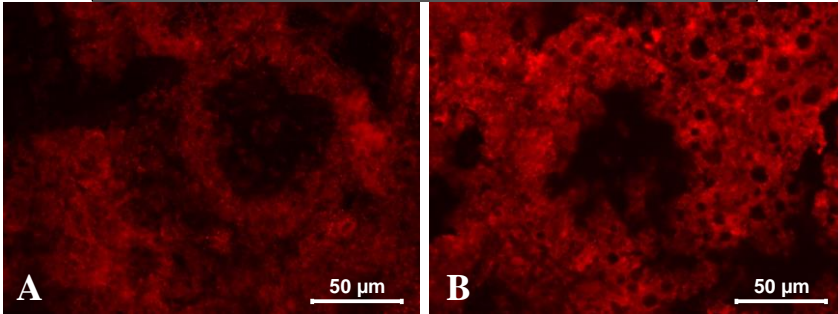
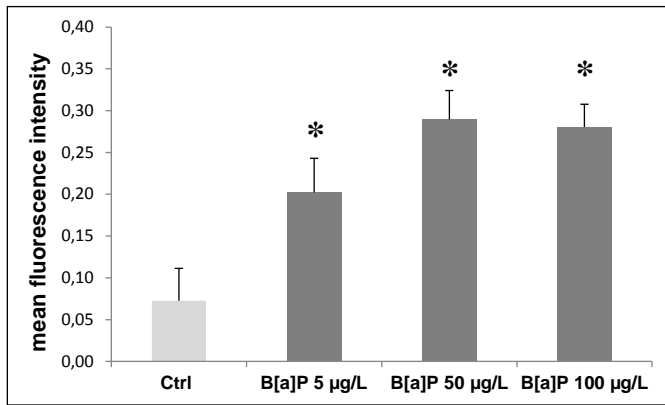
814



815

816 Fig. 4.

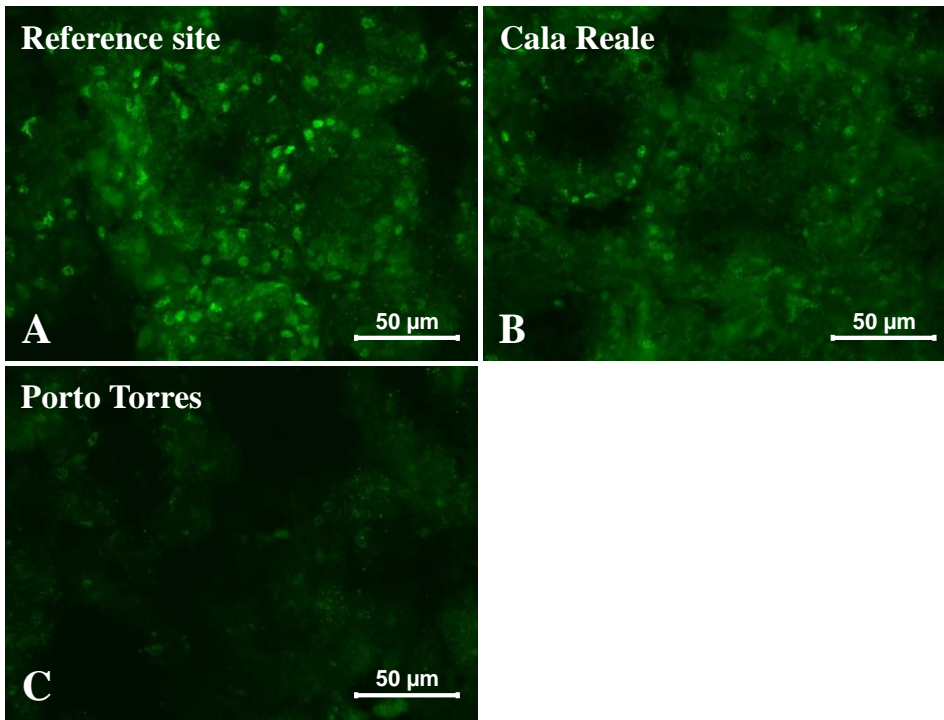
817



818

819 Fig. 5.

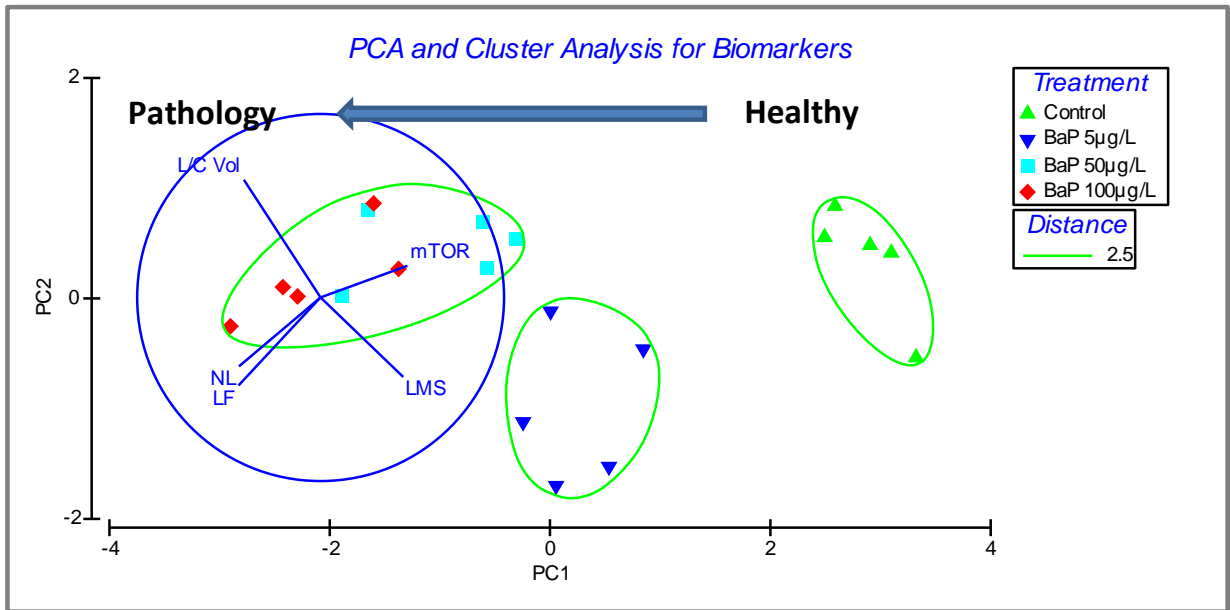
820



821

822 Fig. 6.

823

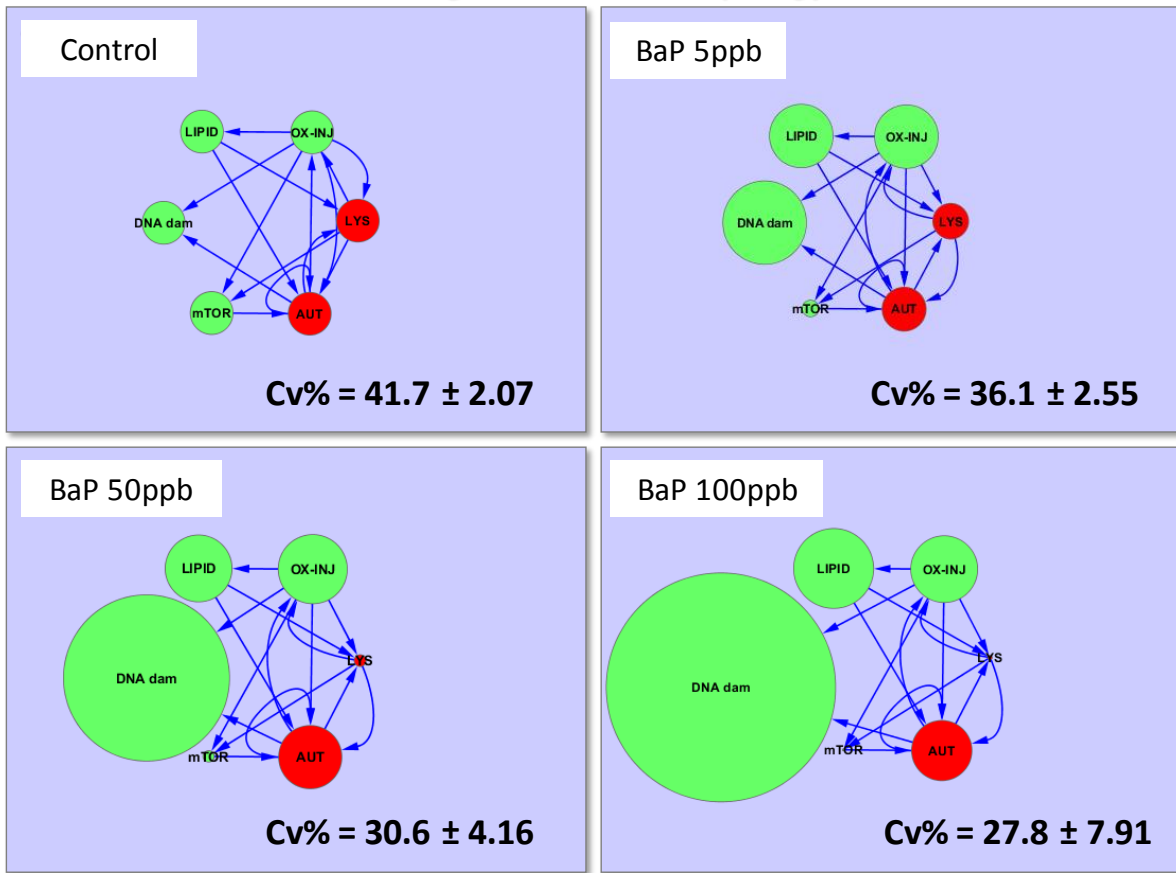


824

825 Fig. 7.

826

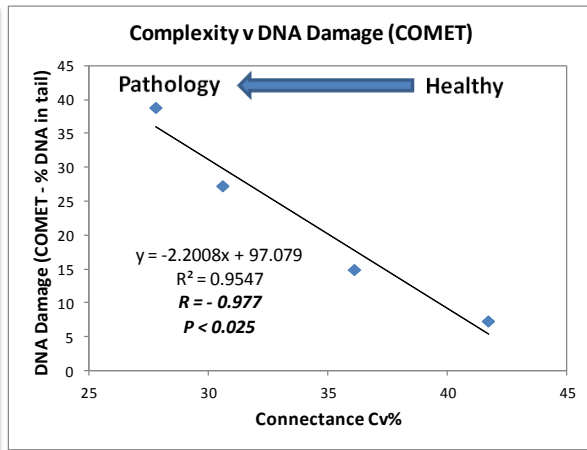
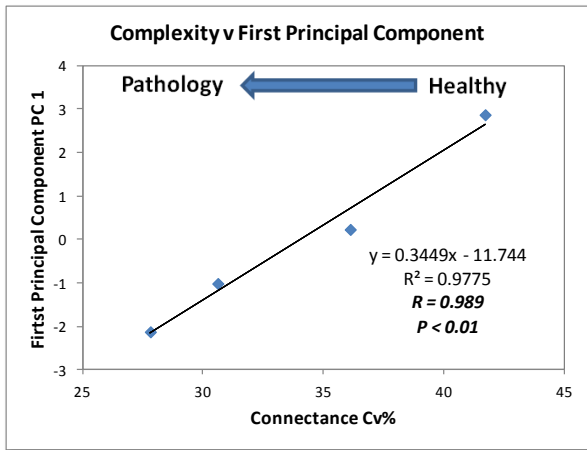
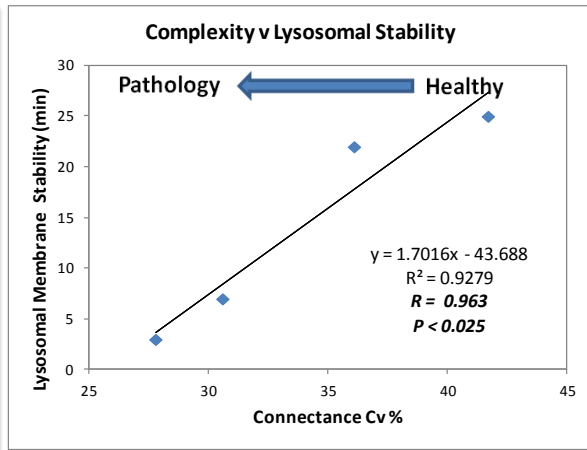
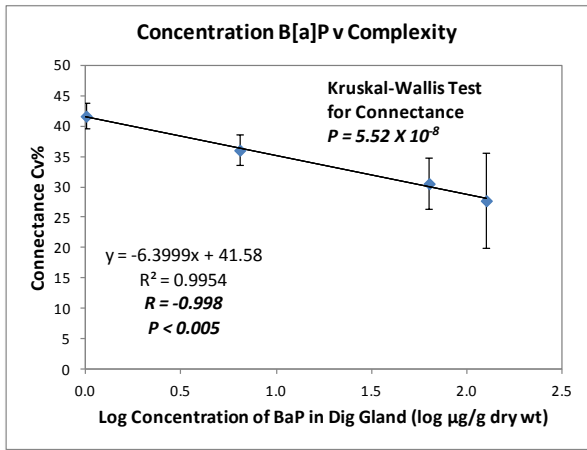
Changes in Network Topology



827

828 Fig. 8.

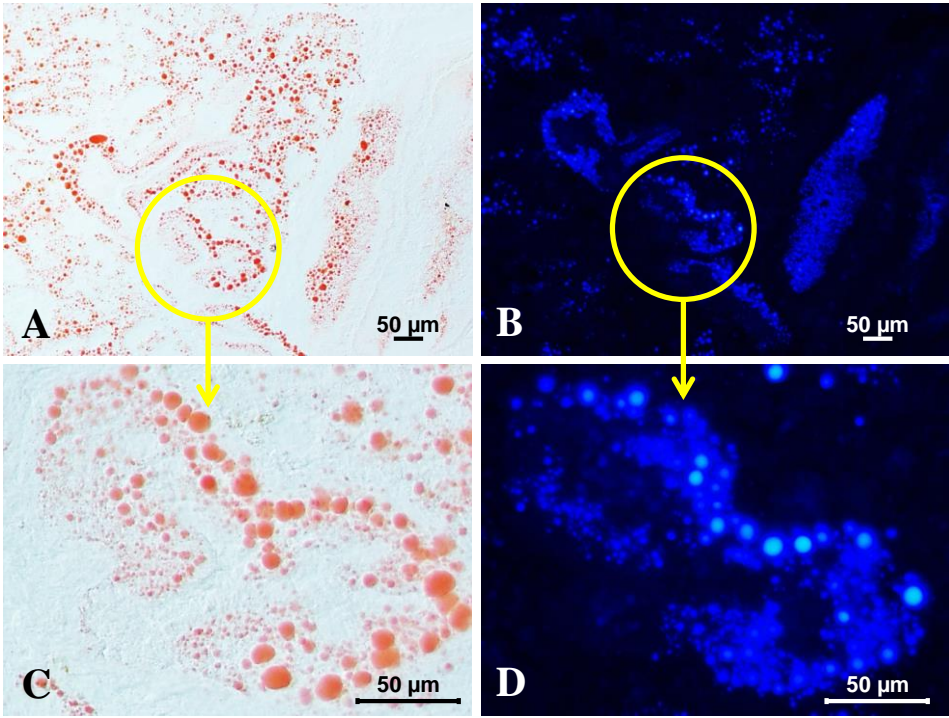
829



830

831 Fig. 9.

832

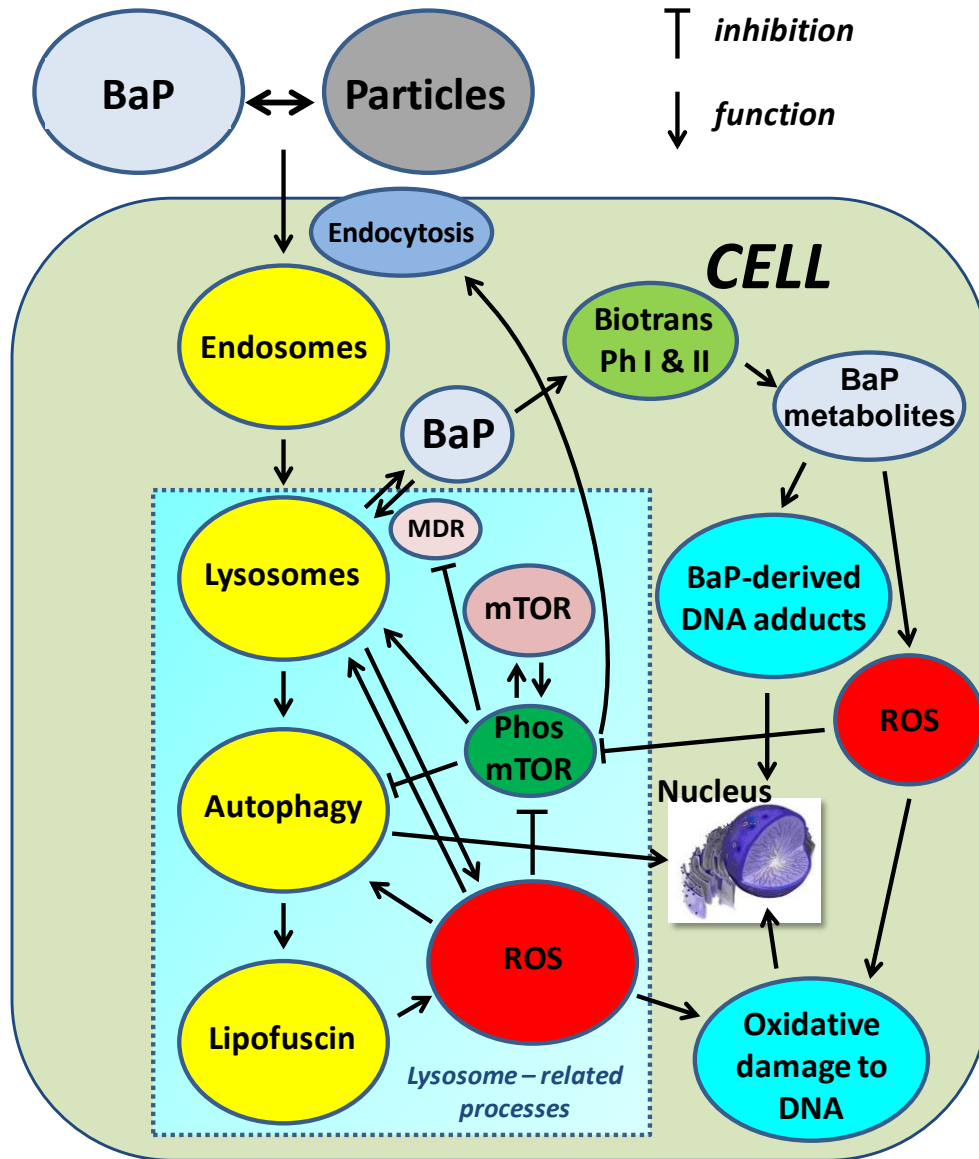


833

834 Fig. 10.

835

Mechanistic model of BaP uptake, intracellular fate and effects



836

837

838 Fig 11.

839

840 Fig. 1. Anti-PAHs immunohistochemical staining (green: FITC conjugated secondary antibody) of
841 digestive gland tissue sections from mussels exposed to different experimental conditions (A:
842 Control; B: 5 µg/L B[a]P; C: 50 µg/L B[a]P; D: 100 µg/L B[a]P). E) Quantitative fluorescence
843 analysis of anti-PAHs immunoreaction. Data are mean ± SD of at least five replicates; * = $p < 0.05$
844 (Mann-Whitney *U*-test). F) Double immunohistochemical staining of digestive glands from mussels
845 exposed to 5 µg/L B[a]P with anti-PAHs and -cathepsin D antibodies (separate colour images for
846 PAHs (FITC, green) and cathepsin D (DyLight594, red) immunoreactivity were merged into a
847 composite image, whereby the colocalization of both antigens in lysosomes of B[a]P exposed
848 mussels was revealed through the coincidence of the two labels resulting in a yellow colour -see
849 arrows and insets).

850

851 Fig. 2. Cryostat unstained sections of digestive glands from mussels exposed to different
852 experimental conditions (A: Control; B: 5 µg/L B[a]P; C: 50 µg/L B[a]P; D: 100 µg/L B[a]P)
853 examined with UV excitation: white-blue fluorescent deposits, in form of droplets, were evident
854 particularly at the higher B[a]P concentrations (C, D) (grayscale images).

855

856 Fig. 3. Lysosomal biomarker responses in digestive gland of mussels exposed to B[a]P (5, 50, 100
857 µg/L). A) Lysosomal membrane stability (cytochemical assay based on acid labilization
858 characteristics of latent hydrolase β-*N*-acetylhexosaminidase); B) lysosomal/cytoplasmic volume
859 ratio (lysosomes reacted for the lysosomal enzyme β-*N*-acetylhexosaminidase: when compared to
860 controls (B1), in mussels exposed to B[a]P an enlargement of autolysosomes was observed (B2),
861 see arrows and insets). Data represent the mean ± SD of at least five replicates. * indicates
862 statistically significant differences ($p < 0.05$ Mann-Whitney *U*-test).

863

864 Fig. 4. Anti-mTOR (phospho S2448) immunohistochemical staining (green: Chromeo conjugated
865 secondary antibody) of digestive gland tissue sections from mussels exposed to different
866 experimental conditions. (A; B) Control (in A separate colour images for mTOR immunoreactivity
867 (Chromeo, green) and the nuclear counterstain propidium iodide (red) were merged into a
868 composite image, whereby the yellow colour highlights the localization of mTOR in perinuclear
869 region of the tubule epithelial cells); C) 5 µg/L B[a]P; D) 50 µg/L B[a]P; E) 100 µg/L B[a]P). (F)
870 Quantitative fluorescence analysis of anti-mTOR immunoreaction. Data are mean ± SD of at least
871 five replicates; * = $p < 0.05$ (Mann-Whitney *U*-test).

872
873 Fig. 5. Quantitative fluorescence analysis of anti-mTOR immunoreaction of digestive gland tissue
874 sections from mussels exposed to B[a]P. Data represent the mean ± SD of at least five replicates. *
875 indicates statistically significant differences ($p < 0.05$ Mann-Whitney *U*-test). Representative
876 images of tissue sections of controls (A) and 50 µg/L B[a]P exposed mussels (B) (red: DyLight594
877 conjugated secondary antibody).

878
879 Fig. 6. Anti-mTOR (phospho S2448) immunohistochemical staining (green: Chromeo conjugated
880 secondary antibody) of digestive gland tissue sections from mussels caged at three sites along the
881 Sardinian coast. A) Reference site (Porto Mannu li Fornelli); B) Cala Reale; D) Porto Torres.

882
883 Fig. 7. Principal component (PCA) and cluster analysis of the biomarker data not including DNA
884 damage. Vectors indicate the directionality of specific biomarkers.

885
886 Fig. 8. Interaction network models based on the physiological and pathological processes
887 represented by the biomarker investigations in mussel digestive cells. Processes represented include
888 lysosomal function, autophagy, mTORC1 signalling, lysosomal lipid accumulation, oxidative injury

889 and DNA damage. Node sizes are based on the proportional change in the biomarker representing
890 the process (see Table 1). System complexity (Connectance $C_v\% \pm 95\% \text{ CL}$, $n = 5$) is shown for
891 each treatment.

892

893 Fig. 9. Statistical modelling for system complexity versus B[a]P concentration (showing $\pm 95\% \text{ CL}$
894 for $C_v\%$, $n = 5$), lysosomal stability, first principal component and DNA damage (COMET).

895

896 Fig. 10. Representative images of cryostat serial sections of digestive glands from mussels exposed
897 to B[a]P 100 $\mu\text{g/L}$ (A, C) stained with Oil-Red O for the evaluation of lysosomal neutral lipid
898 content and (B, D) unstained and analysed with UV excitation, showing that the distribution of the
899 B[a]P fluorescent droplets in the digestive gland cells corresponds to that of the neutral lipid
900 containing vesicles.

901

902 Fig 11. Diagrammatic representation of an explanatory mechanistic framework for the
903 interconnected cellular reactions to B[a]P based on the biomarker data, network modelling and
904 other published sources in the scientific literature. ROS - reactive oxygen species; Phos mTOR -
905 active phosphorylated form of mTORC1 cell signalling system; mTOR - inactive dephosphorylated
906 form of mTORC1; MDR – Pgp40 multidrug transporter; BIOTRANS Ph I & II - Phase I and II
907 biotransformation system (Canova et al., 1998).

908

- 909 -The autophagic process in digestive gland of B[a]P exposed mussels was investigated.
- 910 -B[a]P accumulated in lysosomes/enlarged lipid-rich lysosomes of digestive cells.
- 911 -At higher doses B[a]P overstimulated the autophagy and increased cell catabolism.
- 912 -B[a]P-induced dephosphorylation of mTOR may explain the observed pathological effects.
- 913 -Network connectedness showed that pathology results in a loss of system complexity.
- 914

915 **Supplementary Information**

916

917 *Western blot analysis*

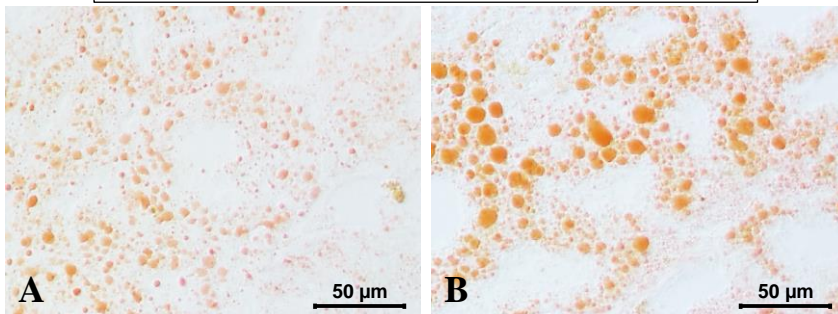
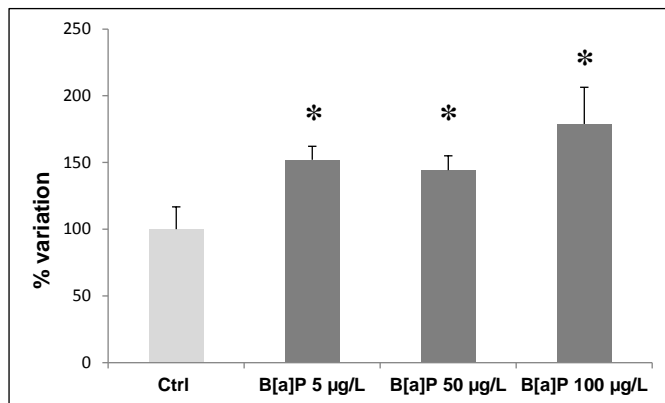
918 Digestive glands were homogenised with NP-40 buffer (150mM sodium chloride, 1% Triton,
919 50mMTris, pH 8.0) containing 1/100 of protease inhibitor cocktail (Sigma-Aldrich) and centrifuged
920 at 1000 rcf for 5 min at 4°C. Pellets were resuspended in the NP-40 buffer and 10 µg of proteins
921 were loaded on a Mini-Protean TGX 4-15% gel (Bio-Rad Laboratories S.r.l) for SDS-PAGE, under
922 reducing conditions. Following electrophoresis, the proteins were transferred onto PVDF
923 membranes in transfer buffer. The membranes were blocked with 5% BSA solution at 4 °C for 1 h.
924 The blots were incubated overnight at 4°C with the primary antibody (anti m-TOR (phospho S2448)
925 antibody, Abcam, ab84400) at 1 ug/ml, followed by incubating with a 1:5000-diluted HRP-
926 conjugated goat anti-rabbit secondary antibody (Bio-Rad Laboratories S.r.l.) for 90 minutes, and
927 then visualized by Clarity™ ECL detection kit. (Bio-Rad Laboratories S.r.l.).

928



930 Fig. S1. Western blot analysis of p-mTOR (S2448) protein indicating that B[a]P induces a
931 dephosphorylation of the protein. Protein bands shown are representative of 3 independent
932 experiments with similar results.

933



934

935 Fig. S2. Lysosomal neutral lipid content in the digestive gland cells of mussels exposed to B[a]P (5,
 936 50, 100 µg/L). Data, expressed as percent change with respect to control values, represent the mean
 937 ± SD of at least five replicates. * indicates statistically significant differences ($p < 0.05$ Mann–
 938 Whitney *U*-test). Representative images of tissue sections from control (A) and B[a]P-exposed
 939 mussels (B) (100 µg/L).